AD-A060 959 TEXAS UNIV AT AUSTIN APPLIED RESEARCH LABS F/G 20/1
MOTION OF GAS BUBBLES IN INTENSE TWO-FREQUENCY SOUND FIELDS.(U)
SEP 78 J R CLYNCH, R A ALTENBURG N00014-76-C-1095
UNCLASSIFIED ARL-TR-78-40 NL

END
DATE FILMED
-79
DDC

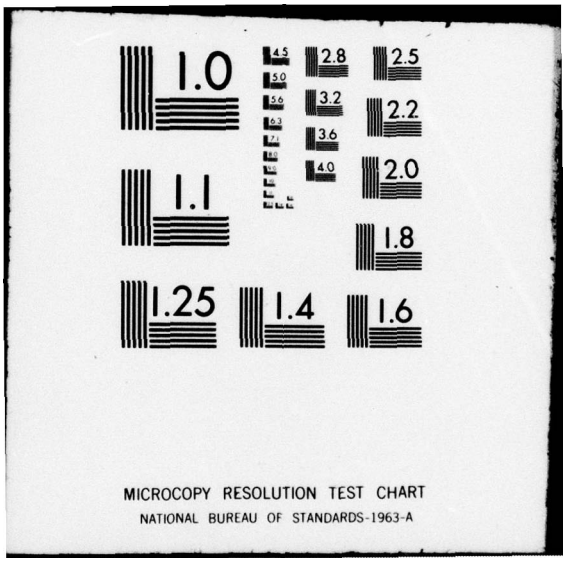
1.0
1.1
1.25
1.4
1.6
1.8
2.0
2.2
2.5
2.8
3.2
3.6
4.0
4.5
5.0
5.6
MICROCOPY RESOLUTION TEST CHART
NATIONAL BUREAU OF STANDARDS-1963-A

LEVEL II

(12)

ARL-TR-78-40

Copy No._____

MOTION OF GAS BUBBLES IN INTENSE TWO-FREQUENCY SOUND FIELDS

Final Report under Contract N00014-76-C-1059

James R. Clynch
Robert A. Apfel

APPLIED RESEARCH LABORATORIES
The University of Texas at Austin
Post Office Box 8029, Austin, Texas 78712

15 November 1978

Sponsored by

Naval Sea Systems Command
Department of the Navy
Washington, D.C. 20362

UNCLASSIFIED

SECURITY CLASSIFICATION

LEVEL II

(12)

REPORT DOCUMENTATION PAGE

READ INSTRUCTIONS BEFORE COMPLETING FORM

1. REPORT NUMBER

2. GOVT ACCESSION NO.

3. RECIPIENT'S CATALOG NUMBER

(9) rept.

4. TITLE (and Subtitle)

(6) MOTION OF GAS BUBBLES IN INTENSE TWO-FREQUENCY SOUND FIELDS,

5. TYPE OF REPORT & PERIOD COVERED

Final, 15 Aug [redacted]76-
14 Aug [redacted]77,

6. PERFORMING ORG. REPORT NUMBER

(14) ARL-TR-78-40

7. AUTHOR(s)

(10) James R. Clynch
Robert A. Altenburg

8. CONTRACT OR GRANT NUMBER(s)

(15) N00014-76-C-1095

9. PERFORMING ORGANIZATION NAME AND ADDRESS

Applied Research Laboratories
The University of Texas at Austin
Austin, TX 78712

10. PROGRAM ELEMENT, PROJECT, TASK AREA & WORK UNIT NUMBERS

11. CONTROLLING OFFICE NAME AND ADDRESS

(11) Office of Naval Research
Physics Program Office
Arlington, VA 22217

12. REPORT DATE

12 Sept[redacted]78

13. NUMBER OF PAGES

65 (12) 61p.

14. MONITORING AGENCY NAME & ADDRESS (if different from Controlling Office)

15. SECURITY CLASS. (of this report)

UNCLASSIFIED

15a. DECLASSIFICATION/DOWNGRADING SCHEDULE

16. DISTRIBUTION STATEMENT (of this Report)

Approved for public release; distribution unlimited.

17. DISTRIBUTION STATEMENT (of the abstract entered in Block 20, if different from Report)

18. SUPPLEMENTARY NOTES

19. KEY WORDS (Continue on reverse side if necessary and identify by block number)

bubble dynamics
cavitation
nonlinear acoustics

20. ABSTRACT (Continue on reverse side if necessary and identify by block number)

(U) The radial motion of gas bubbles in water driven by an intense sound field containing two closely spaced frequency components has been studied via numerical integration of the equation of motion. The small driving amplitude perturbation theory solution is developed for comparison with the numerical results. Emphasis is placed on the secondary frequency component at the difference of the driving frequencies which is generated by the nonlinear motion of the bubble. → next page

DD FORM 1 JAN 73 1473 EDITION OF 1 NOV 65 IS OBSOLETE

404 434

UNCLASSIFIED

SECURITY CLASSIFICATION

20. (Cont'd)

(U) Cases where the natural resonance frequency of the bubble is much greater than, approximately equal to, and less than the driving frequencies are discussed. Acoustic driving pressures of 0.1 bar to 1.5 bar were used in an ambient pressure of 1.0 bar. The spectrum of the radial motions has been extensively examined and many examples are shown in this report.

(U) Agreement between perturbation theory predictions and the numerical integration is good for the first and second order terms up to driving pressures of 0.25 bar in all cases. All cases show many very narrow lines at the lower driving pressures. Broadband noise generated by collapsing bubbles eventually obscures these lines.

(U) At moderate to high driving pressures the difference frequency component is larger than the perturbation theory prediction, especially for the case of the driving frequencies being below resonance. This suggests that larger bubbles driven at moderate levels may be the most useful in enhancing the nonlinearity of water although tradeoffs involving scattering would have to be examined in each particular case.

TABLE OF CONTENTS

LIST OF FIGURES

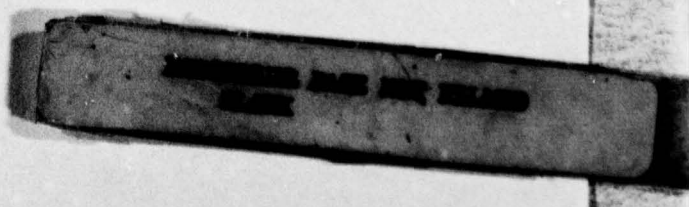

LIST OF TABLES

I. INTRODUCTION

This is the final report, under Contract N00014-76-C-1095, of a study of the response of small air bubbles in water to intense, multifrequency acoustic waves. The approach was to numerically integrate the equation of motion of a bubble using a variety of bubble sizes and acoustic driving pressures. Because the numerical integration required considerable computer time, only a limited number of cases was studied.

Basically, this is a study in bubble dynamics, similar to studies conducted by Flynn[1] and many others.[2] The impetus for the study, however, came from the field of nonlinear acoustics. Westervelt[3] had proposed and Muir and Blue[4] had confirmed that large amplitude sound waves containing two frequencies interact in water to produce secondary sound waves at the sum and difference frequencies. This process is highly inefficient. However, if microscopic bubbles are introduced into the water, the nonlinearity of the medium increases.[5-8] The possibility therefore exists that the efficiency of nonlinear generation of low frequency sound can be improved without seriously degrading all of the process's favorable features.[9] While experimental work[8, 10-13] has verified that this principle operates, most of this work has focused on acoustic measurements and little is known about bubble size distributions and/or bubble densities. The present study was undertaken to partially bridge the gap between theory and experiment.

The method of this study was to numerically integrate the equation of motion of a spherical bubble in a high intensity sound field consisting of two frequencies. Experimental conditions described in Refs. 10 and 12 were modeled. While the motion of a single bubble will not yield numbers which can be directly compared to the experimental data, examination of the motions of bubbles of various sizes can show which sizes are important in the radiation of sound at the difference of the driving frequencies.

This study determines the limits where perturbation theory is valid and indicates quantitatively how results obtained from an exact solution differ from those obtained from perturbation theory at high pressures in complex driving fields.

An outline of the theory of bubble motion, including the perturbation theory solution with two driving frequencies, is given in section II. The numerical integration program and the data base it produced are discussed in section III. The results are presented in section IV, where three cases are examined in detail; a summary is given in section V.

II. THEORETICAL BACKGROUND

The motion of a bubble in an infinitesimal amplitude sound field is fairly simple: the bubble oscillates at the driving frequency. However, the case of bubbles moving under a large driving pressure is much more complex. Above a driving pressure threshold, the bubbles can go into an almost complete collapse as the momentum of the in-flowing water overcomes the increasing pressure of the compressed gas within the bubble. During these collapses the radius reduces to a very small fraction of its equilibrium value. The precise form this collapse takes depends on the equation of state of the very hot gas within the collapsed bubble and is not well understood.

The situation with a single frequency intense sound field has been studied extensively both analytically[1,14] and numerically.[15,16]. The two-frequency case, however, is more difficult to study because of its complexity. Analytical methods, other than in the small amplitude limit where perturbation theory can be applied, do not appear very fruitful. Therefore, "the differential equation" for the bubble motion has been studied numerically. There are, in fact, several differential equations which are used. The four most common ones[1] are shown in Fig. 1: (1) Noltingk-Neppiras - assumes an incompressible fluid; (2) acoustic approximation - based on allowing for a fixed, finite speed of sound; (3) Herring-Flynn - based on a better accounting of energy storage on compression; and (4) Kirkwood-Bethe - based on specific enthalpy and allowing for the speed of sound to vary with position and time. These various approaches are alternative approximations to the equation of state of the fluid. All give essentially the same result except in the final phase of bubble collapse. To study the broadband high frequency shock waves generated by bubble collapse, the Kirkwood-Bethe equation is required. In addition to an assumption about the equation of state of the fluid, an equation of state for the gas must be assumed. Most investigators

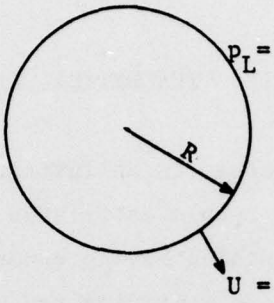

p_∞ = Pressure in Fluid Far from Wall

ρ_o = Fluid Ambient Density

c_o = Small Signal Speed of Sound

μ = viscosity

IMCOMPRESSIBLE FLUID : NOLTINGK-NEPPIRAS

$$R\dot{U} + \frac{3}{2} U^2 = \frac{1}{\rho_o} [p_L - p_\infty]$$

ACOUSTIC APPROXIMATION:

$$R\dot{U} + \frac{3}{2} U = \frac{1}{\rho_o} [p_L - p_\infty + \frac{R}{c_o} (1 - \frac{U}{c_o}) \dot{p}_L]$$

HERRING-FLYNN EQUATION:

$$(1 - 2\frac{U}{c_o}) R\dot{U} + (1 - \frac{4}{3}\frac{U}{c_o}) \frac{3}{2} U^2 = \frac{1}{\rho_o}[p_L - p_\infty + \frac{R}{c_o} (1 - \frac{U}{c_o}) \dot{p}_L - \frac{4\mu U}{R}]$$

KIRKWOOD-BETHE EQUATION:

$$(1 - \frac{U}{c}) R\dot{U} + (1 - \frac{U}{3c}) \frac{3}{2} U^2 = (1 - \frac{U}{c}) H + \frac{U}{c} (1 - \frac{U}{c}) R \frac{dH}{dR}$$

$$H \equiv \int_{p_\infty}^{p(R)} \frac{dp}{\rho} = \text{specific enthalpy of fluid at bubble wall}$$

c = Local speed of sound

FIGURE 1

BUBBLE DYNAMICS DIFFERENTIAL EQUATIONS

AS-78-1376
JRC 1095

to date have assumed either isothermal or adiabatic conditions for the gas with a specified ratio of specific heats. (Epstein[17] has done some work with adiabatic cases where the ratio of specific heats, γ, takes on a second value during the final stages of collapse.) This study has considered only adiabatic motion.

Whereas this study concentrated on numerical integration of the acoustic approximation equation and not on analytical methods, a perturbation solution for the small amplitude case is useful for comparison purposes. The differential equation considered is

$$R\ddot{R} + \frac{3}{2}\dot{R}^2 = \frac{1}{\rho_o}\left[p_L - p_\infty + \frac{R}{c_o}\left(1 - \frac{\dot{R}}{c_o}\right)\dot{p}_L - \frac{4\mu R}{R}\right] \quad , \tag{1}$$

where

R is the bubble radius,

ρ_o is the water density,

p_L is the pressure at the bubble wall,

p_∞ is the ambient pressure,

c_o is the ambient sound speed,

μ is the viscosity of water,

one dot indicates differentiation with respect to time, and two dots indicate a double differentiation with respect to time. The driving acoustic field, p_a, will be contained in

$$p_L = p_b + p_a \quad , \tag{2}$$

where

$$p_a = p_1 \sin\omega_1 t + p_2 \sin\omega_2 t \quad , \tag{3}$$

$$p_b = p_\infty\left(\frac{R_o}{R}\right)^{3\gamma} + \frac{2\sigma}{R} \quad . \tag{4}$$

In the above equations, p_b is the gas pressure in the bubble and consists of the compression term and a term involving the surface tension σ. The value of the adiabatic exponent, γ, could be set arbitrarily in the computer program. In this way adiabatic (γ=5/3) or isothermal (γ=1) approximations were made. R_o is the equilibrium bubble size in the absence of an acoustic sound field and the driving acoustic pressures at angular frequencies ω_1 and ω_2 are p_1 and p_2, respectively.

To obtain the simplest infinitesimal motion approximation, one can examine

$$R\ddot{R} + \frac{3}{2}\dot{R}^2 = \frac{1}{\rho_o}\left\{ p_\infty\left[1 - \left(\frac{R_o}{R}\right)^{3\gamma}\right] + p_a\right\} \quad , \tag{5}$$

and let

$$\frac{R}{R_o} = 1 + x \quad , \tag{6}$$

where x is a small number. If only one driving frequency is used, then the equation in x to first order would be

$$\ddot{x} + \frac{3\gamma p_\infty}{\rho_o R_o^2}\, x = \frac{p_1 \sin\omega_1 t}{\rho_o R_o^2} \quad . \tag{7}$$

The natural bubble resonance frequency, ω_o, in this approximation is given by

$$\omega_o^2 = \frac{3\gamma p_\infty}{\rho_o R_o^2} \quad , \tag{8}$$

and

$$x = x_{o1} \sin\omega_1 t \quad , \tag{9}$$

with

$$x_{01} = \frac{p_1}{\rho_o R_o^2(\omega_o^2-\omega_1^2)} = \frac{1}{3\gamma}\left(\frac{\omega_o^2}{\omega_o^2 - \omega_1^2}\right)\frac{p_1}{p_\infty} \quad . \tag{10}$$

For two driving frequencies, the perturbation theory solution to first order is

$$x = x_{01}\sin\omega_1 t + x_{02}\sin\omega_2 t \quad , \tag{11}$$

with x_{01} and x_{02} given by Eq. (10) with appropriate subscripts. This solution may then be used in an approximation to the equation of motion which contains terms of second order.

At this point one must decide on the relative size of $x_{01,02}$ and $R_o/\lambda_{1,2}$ where $\lambda_{1,2}$ are the wavelengths at $\omega_{1,2}$. If the bubble is so small that x_{01} is larger than this ratio, the terms containing $R_o\dot{p}_a/c_o$ and $\dot{x}R_o/c_o$ may be ignored; otherwise they must be retained. For simplicity these terms will be dropped since we are looking only for an illustrative solution.

Letting

$$x = x_F + x_s \quad , \tag{12}$$

x_F being the first order solution and x_s the second order term, the equation of motion becomes

$$(1+x)\ddot{x} + \omega_o^2 x = \left\{\frac{1}{\rho_o R_o^2}(p_1\sin\omega_1 t + p_2\sin\omega_2 t)\right\} - \frac{3}{2}\dot{x}^2 - \omega_o^2\frac{(3\gamma+1)}{2}x^2 \quad . \tag{13}$$

The term in braces on the right-hand side of Eq. (13) is balanced by x_F from the left-hand side, leaving

$$\ddot{x}_s + \omega_o^2 x_s = -x_F\ddot{x}_F - \frac{3}{2}\dot{x}_F^2 + \omega_o^2\left(\frac{3\gamma+1}{2}\right)x_F^2 \quad , \tag{14}$$

or

$$\ddot{x}_s + \omega_o^2 x_s = x_{01}^2 \left\{ \left[\frac{\omega_1^2}{2} + \left(\frac{3\gamma+1}{4} \right) \omega_o^2 \right] \left[1 + \cos(2\omega_1 t) \right] \right.$$
$$\left. - \frac{3}{4} \omega_1^2 \left[1 - \cos(2\omega_1 t) \right] \right\}$$
$$+ x_{02}^2 \left\{ \left[\frac{\omega_2^2}{2} + \left(\frac{3\gamma+1}{4} \right) \omega_o^2 \right] \left[1 + \cos(2\omega_2 t) \right] \right.$$
$$\left. - \frac{3}{4} \omega_2^2 \left[1 - \cos(2\omega_2 t) \right] \right\} \qquad (15)$$
$$+ x_{01} x_{02} \left\{ \left[\frac{\omega_1^2 + \omega_2^2}{4} - \left(\frac{3\gamma+1}{2} \right) \omega_o^2 \right] \left[\cos(\omega_1+\omega_2)t + \cos(\omega_1-\omega_2)t \right] \right.$$
$$\left. - \frac{3}{2} \omega_1 \omega_2 \left[\cos(\omega_1-\omega_2)t - \cos(\omega_1+\omega_2)t \right] \right\} .$$

This expression contains all of the essential features of a more complete development for infinitesimal waves. A simple harmonic oscillation is driven by terms at 0 Hz, $2\omega_1$, $2\omega_2$, $\omega_1+\omega_2$, and $\omega_1-\omega_2$. This perturbation theory development is incorrectly handling the 0 Hz term. The other forcing terms should be meaningful at low driving pressures when all frequencies are far from resonances. The terms arising from the $\dot{R}^2$ and $R\ddot{R}$ in Eq. (1) are included here but were absent from the analytical development by Rolleigh and Clynch.[10] In that development the bubbles were assumed very small and consequently ω_o was assumed much larger than all other frequencies in the problem. In the current study these assumptions were not made and therefore these terms have been kept.

A diagram of the frequencies studied is shown in Fig. 2. In this diagram, f_o is the bubble resonance frequency,

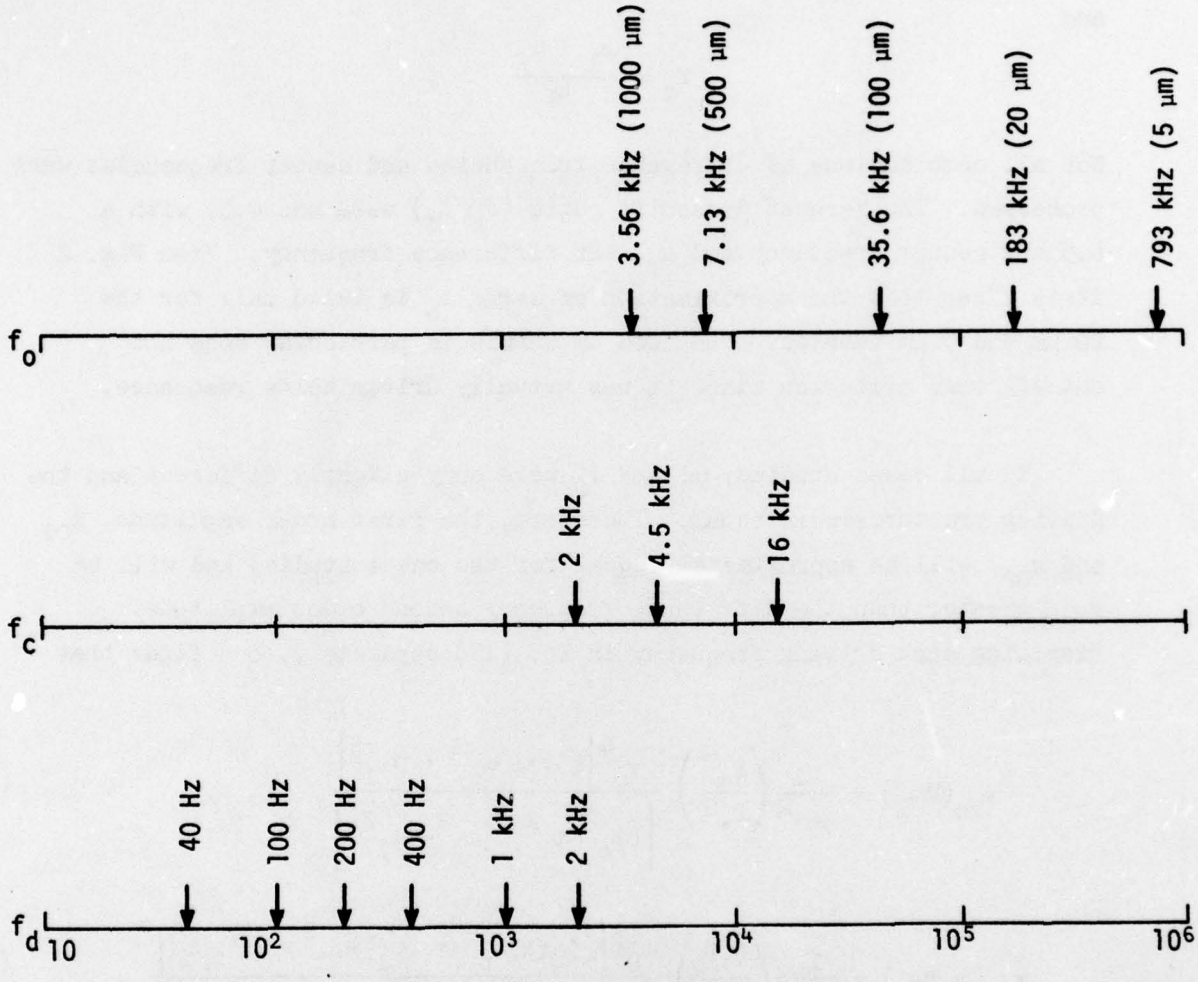

FIGURE 2

FREQUENCIES USED IN STUDY

Difference Frequency f_c Center Frequency f_c

Bubble Resonance Frequency f_o (Bubble radius in brackets)

AS-78-1377
JRC 1095

$$f_d = \frac{\omega_1 - \omega_2}{2\pi} \quad , \tag{16}$$

and

$$f_c = \frac{\omega_1 + \omega_2}{4\pi} \quad . \tag{17}$$

Not all combinations of difference frequencies and center frequencies were processed. The largest downshift ratio (f_c/f_d) used was 4.5, with a 4.5 kHz center frequency and a 1 kHz difference frequency. From Fig. 2 it is clear that the approximation of large ω_o is valid only for the 20 μm and 5 μm bubbles. The 1000 μm bubble in particular does not satisfy this criterion since it was actually driven below resonance.

In all cases studied, ω_1 and ω_2 were only slightly different and the driving pressures were equal. Therefore, the first order amplitude, x_{01} and x_{02}, will be approximately equal for the cases studied and will be much greater than the difference frequency second order amplitude. Examining each driving frequency in Eq. (15) separately, one finds that

$$x_{so}(2\omega_1) = \frac{1}{36\gamma^2}\left(\frac{p_1^2}{p_\infty^2}\right) \frac{\omega_o^4\left[(3\gamma+1)\omega_o^2 + 5\omega_1^2\right]}{\left[(\omega_o^2-\omega_1^2)^2(\omega_o^2-4\omega_1^2)\right]} \quad , \tag{18}$$

$$x_{so}(\omega_1+\omega_2) = \frac{1}{18\gamma^2}\left(\frac{p_1 p_2}{p_\infty^2}\right) \frac{\omega_o^4\left[(3\lambda+1)\omega_o^2 + (\omega_1^2+\omega_2^2) + 3\omega_1\omega_2\right]}{\left[(\omega_o^2-\omega_1^2)(\omega_o^2-\omega_2^2)(\omega_o^2-(\omega_1+\omega_2)^2)\right]} \quad , \tag{19}$$

$$x_{so}(\omega_1-\omega_2) = \frac{1}{18\gamma^2}\left(\frac{p_1 p_2}{p_\infty}\right) \frac{\omega_o^4\left[(3\gamma+1)\omega_o^2 + (\omega_1^2+\omega_2^2) - 3\omega_1\omega_2\right]}{\left[(\omega_o^2-\omega_1^2)(\omega_o^2-\omega_2^2)(\omega_o^2-(\omega_1-\omega_2)^2)\right]} \quad , \tag{20}$$

and $x_{so}(2\omega_2)$ can be obtained from Eq. (18) by substituting ω_2 for ω_1. The equation for ω_o has been used to put these equations in the form of dimensionless ratios. While these equations can give qualitative results away from resonances and low driving pressures, they are really not applicable at the acoustic pressures usually present in experiments.

For an ω_o that is much larger than any of other frequencies involved, these equations reduce to the results of Rolleigh and Clynch.[10] In that limit the amplitudes of the bubble radial oscillations at the sum and difference frequencies are equal and are twice the value at each second harmonic. Thus, in the large ω_o limit, the amplitude oscillations at the secondary frequencies are partitioned into three equal parts: at the sum frequency, at the difference frequency, and at both the second harmonics. However, this partition will not apply to the radiated sound field. The sound radiated will be proportional to the second time derivative of the volume oscillation, causing each frequency component of the sound to be weighted by the frequency squared.

In the general case, the equations are quite complex. Even though they apply only at small acoustic pressures, they can serve as a guide to frequency dependencies. In addition to examining absolute levels, the ratios of x_{so}'s to the values computed by numerical integration will be compared to provide an estimate of when the perturbation theory solution can be used to predict spectral shape.

III. STUDY PROCEDURE

The motion of a gas bubble in a two-frequency intense sound field was investigated through numerical integration of an equation of motion. The equation integrated by the computer was the acoustic approximation with viscosity added:

$$R\ddot{R} + \frac{3}{2}\dot{R}^2 = \frac{1}{\rho_o}\left\{P_L - P_\infty + \frac{R}{c_o}\left(1 - \frac{\dot{R}}{c_o}\right)\dot{P}_L - \frac{4\mu\dot{R}}{R}\right\} \quad . \tag{21}$$

The output, which was unevenly spaced in time, was first placed on magnetic tape and then was interpolated to produce an even time grid which was Fourier transformed. The output of the fast Fourier transforms (FFT's) was placed on magnetic tapes and plotted. (The capability to plot time histories of bubbles also exists.)

A. The Integration Program

Equation (21) was integrated by program GASBUBL5 on the CDC 3200 computer at Applied Research Laboratories, The University of Texas at Austin (ARL:UT). This program accepts control cards which define the characteristics of the bubbles, the ambient fluid, the driving sound field, the initial conditions, and the time interval to integrate. The equation of motion was then integrated using a fourth order Runge-Kutta algorithm. This integration procedure was chosen because it allows the step size to vary. The output from GASBUBL5 is a magnetic tape containing the times, radii, and the first and second time derivatives of R.

The integration time step was varied automatically in the program. An absolute maximum time step of one hundredth of the smallest period (bubble resonance period or driving sound period) was used. A convergence criterion on the change in bubble radius was applied after each step. If this test

is failed, the program backed up one step and halved the step. If the convergence criterion is failed twice consecutively, a major restart was done. In this case the program backed up 20 steps, reduced the time step by a factor of 10, and continued. A circular buffer of the 100 previous points was kept to allow for five overlapping major reductions. Only after a point was 100 calculations old was it moved from the circular buffer to storage for output to magnetic tape. Major reductions in step size were also triggered by a negative bubble radius.

A problem was encountered with this algorithm in the case of 5 μm bubbles undergoing collapse. The step size was constantly being reduced to the point where accumulated round-off error made the calculation meaningless. Therefore, when the step size became less than 10^{-90} sec, the step size was reset at 10^{-90} sec and kept there.

In addition to being reduced automatically, the step size was automatically doubled if 20 steps of the same size occurred. If the resulting step size was greater than the absolute maximum, the maximum was used.

To validate the program, the curves given by Flynn[1,15] were recalculated. This was done for both adiabatic and isothermal conditions. In both cases the GASBUBL5 curves were in excellent agreement with those of Flynn.

B. Data Base

Center driving frequencies and difference frequencies which matched experimental data on hand were chosen for study. A wide range of bubble sizes (5 μm to 1000 μm) was used to include cases where the resonance was above, nearly equal to, and below the same driving frequency. Pressures of 0.1 bar, where the perturbation theory should hold, to 1.5 bars, where the perturbation theory certainly will not hold, were used.

Table I is a summary of the cases that were integrated. In each case marked with an X, the full set of pressures was run. Each integration with two-frequency data was run out to a time corresponding to 100 difference frequency periods. All integrations began with the bubble at rest. In all cases an adiabatic exponent of 5/3 was used.

TABLE I

SUMMARY OF DATA BASE

f_c(kHz)	2					4.5					16				
f_d(Hz)	0	40	100	200	400	0	100	200	400	1000	0	200	400	1000	2000
Bubble Size (μm) 1000	X	X	X	X	X	X	X	X	X	X	X	X	X	X	X
500	X		X		X	X			X		X		X		X
100	P		P		P	X	X		X		X		X		X
20	X		X		X	X	X		X		X		X		X
5	X				X	X			X		X		X		X

Items marked with X have pressures of 0.1, 0.25, 0.50, 1.0, and 1.5 bars complete.

Items marked with P are partially complete.

IV. RESULTS OF THE NUMERIC INTEGRATIONS

A thorough analysis of all the integration results has not yet been made. Three illustrative cases will be examined which shed light on the motion of bubbles in a complex high pressure sound field. In all cases an adiabatic equation of state (γ=5/3) for an ideal gas was used. The ambient pressure was taken at 1.0 bar, the surface tension was 75 dynes/cm, and the viscosity was 0.01 poise.

All the cases considered had a difference frequency of 400 Hz. Two bubbles were used. (1) A 20 μm bubble with a resonance of 183 kHz is illustrative of the small bubble, high frequency resonance case. (2) A 500 μm bubble (7.13 kHz resonance) was used with two sets of driving frequencies: one where the frequencies are on the order of the resonance frequency (4.3 kHz and 4.7 kHz) and the other where the frequencies are above the resonance frequency (15.8 kHz and 16.2 kHz).

A. Small Bubbles ($f_o \gg f_1, f_2$)

As an example of a small bubble case, a 20 μm bubble driven at 4.3 kHz and 4.7 kHz is considered. In the present context "small" is taken to mean small enough that the resonance frequency (which is inversely proportional to the equilibrium radius) is much greater than the other frequencies. In this case, the f_o is 183 kHz and easily satisfies this criterion. It should be noted, however, that the surface tension contribution to the internal pressure at equilibrium is only 0.075 bars. Therefore this is still a very compliant bubble.

The Fourier transform of the normalized bubble radial motion, x, for a drive pressure of 0.1 bar per primary ($\xi_1=\xi_2=0.1$) is shown in Fig. 3. Here $\xi_i=P_i/P_\infty$. The most obvious feature of this figure is the narrowness of the lines. In fact, the lines are narrower than a resolution cell and a true estimate of the line level must allow for the fact that part of the energy shows up in sidebands for any finite FFT

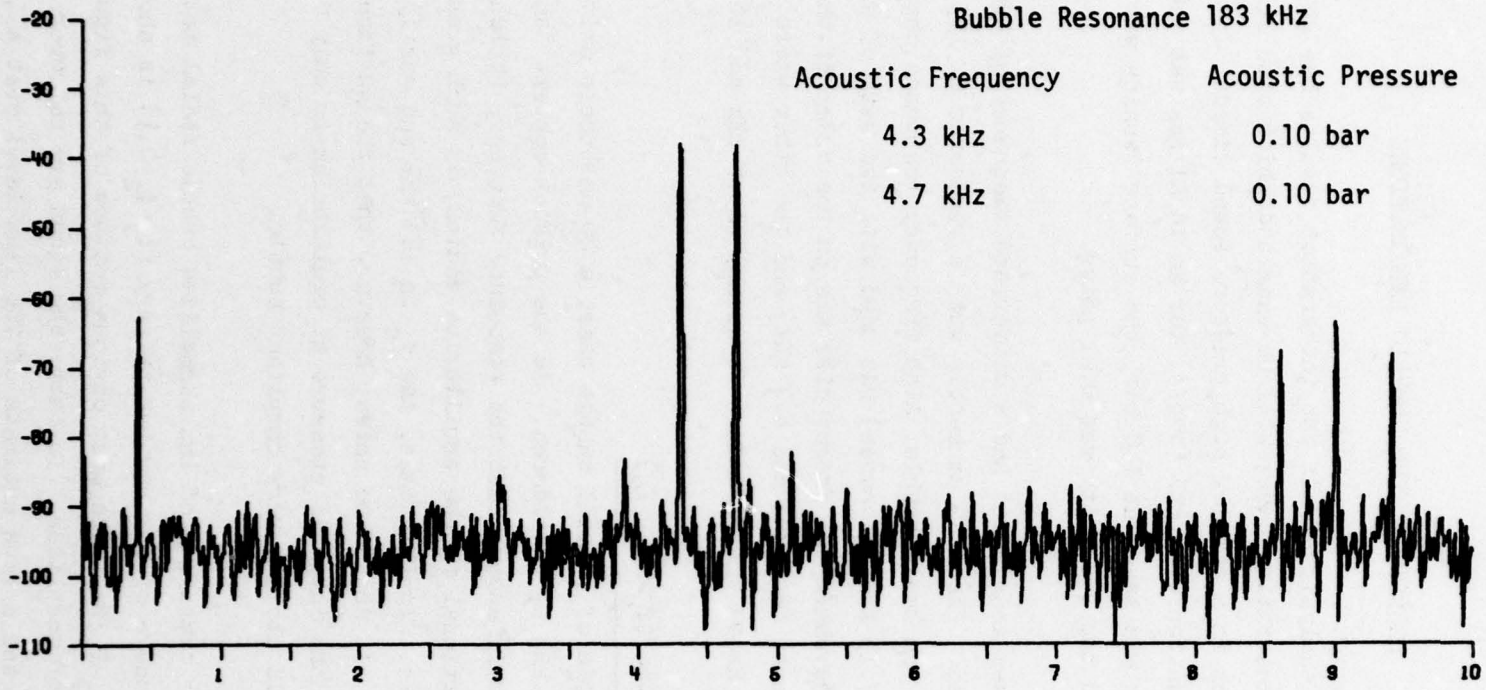

FIGURE 3

RADIAL MOTION SPECTRUM OF 20 μm BUBBLE

AS-78-1378
JRC 1095

if the line is not exactly in the cell center. A Hanning window has been applied to these transforms to minimize this effect, but it is still present.

The two lines of the drive frequencies appear to be at -37 dB from a measurement of the levels in Fig. 3. A more exact value using the adjacent cell values gives -34.4 dB, in excellent agreement with Eq. (10) which predicts -34.0 dB. In addition to the lines at the driving frequencies, second order lines at the difference frequency of 400 Hz and at frequencies of $2f_1$, $2f_2$, and f_1+f_2 are shown. As predicted by Eqs. (18) and (19) and discussed in section II, the energy in the latter three lines is divided evenly between the two second harmonics on the one hand and the sum frequency on the other. The spectrum of x on an expanded frequency scale is shown in Fig. 4. Here third order mixing effects show up as lines around $3f_c$ and also as sidebands on the main line at the driving frequencies. The exact general perturbation solution for these lines has not been presented here, but in the limit of $f_o > f_1$, f_2, the central line should be

$$60 \log(\xi) - 20 \log\left\{(3\gamma)\left(\frac{3\gamma+1}{2}\right)\left(\frac{3\gamma+2}{3}\right)\right\} = -85 \text{ dB} \quad ,$$

which appears to be in good agreement with Fig. 4.

A list of all first and second order line levels and the perturbation theory predictions is given in Table II for these driving frequencies and this bubble. Results for two higher driving pressures are also shown. The perturbation theory results are remarkably accurate at ξ of 0.25 but diverge from the integrated results at 0.5 bar driving pressure.

The spectrum of the 0.25 bar driving pressure is shown in Figs. 5 through 7. The higher order terms are present through many orders as shown in Fig. 6. It is interesting that the first and second order terms are predicted so accurately when so many higher orders have a significant amount of energy. Figure 7 shows this spectrum to a much higher frequency

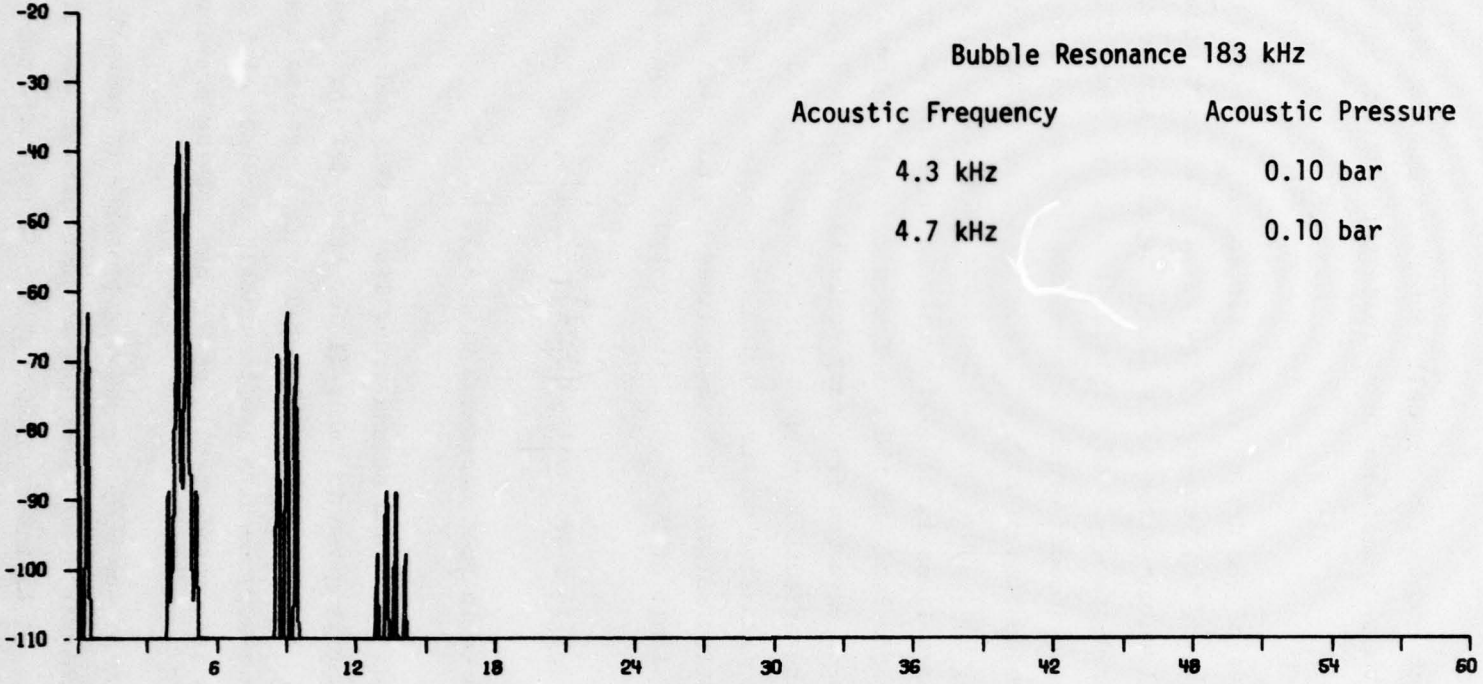

FIGURE 4

RADIAL MOTION SPECTRUM OF 20 μm BUBBLE

AS-78-1379
JRC 1095

TABLE II

SMALL BUBBLE CASE
COMPARISON OF INTEGRATION RESULTS AND PERTURBATION THEORY

Values of x in decibels

Pressure	0.1 bar/primary			0.25 bar/primary			0.5 bar/primary		
Frequency	0	PT	0 - PT	0	PT	0 - PT	0	PT	0 - PT
f_1	-34.4	-34.0	-0.4	-26.0	-26.0	0.0	-16.7	-20.0	3.3
f_2	-34.4	-34.0	-0.4	-26.0	-26.0	0.0	-16.8	-20.0	3.2
$2f_1$	-65.2	-64.4	-0.8	-48.2	-48.4	0.2	-28.2	-36.4	8.2
$2f_2$	-65.2	-64.4	-0.8	-48.1	-48.4	0.3	-28.2	-36.4	8.2
$f_1 + f_2$	-59.2	-58.4	-0.8	-42.4	-42.4	0.0	-24.5	-30.4	5.9
$f_2 - f_1$	-59.2	-58.4	-0.8	-42.4	-42.4	0.0	-21.2	-30.4	9.2

R_o = 20 μm f_o = 183 kHz

f_1 = 4.3 kHz f_2 = 4.7 kHz

0 = Integrated Results

PT = Perturbation Theory

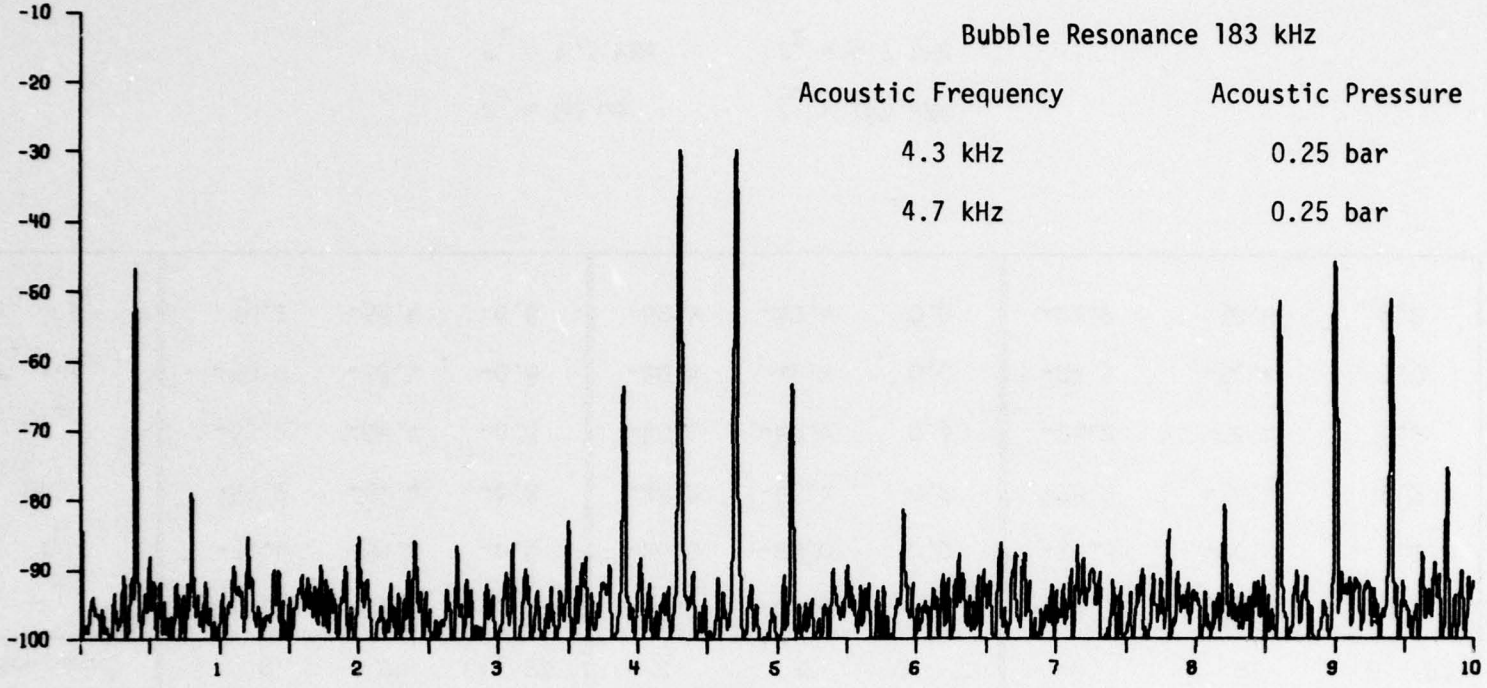

FIGURE 5

RADIAL MOTION SPECTRUM OF 20 μm BUBBLE

AS-78-1380
JRC 1095

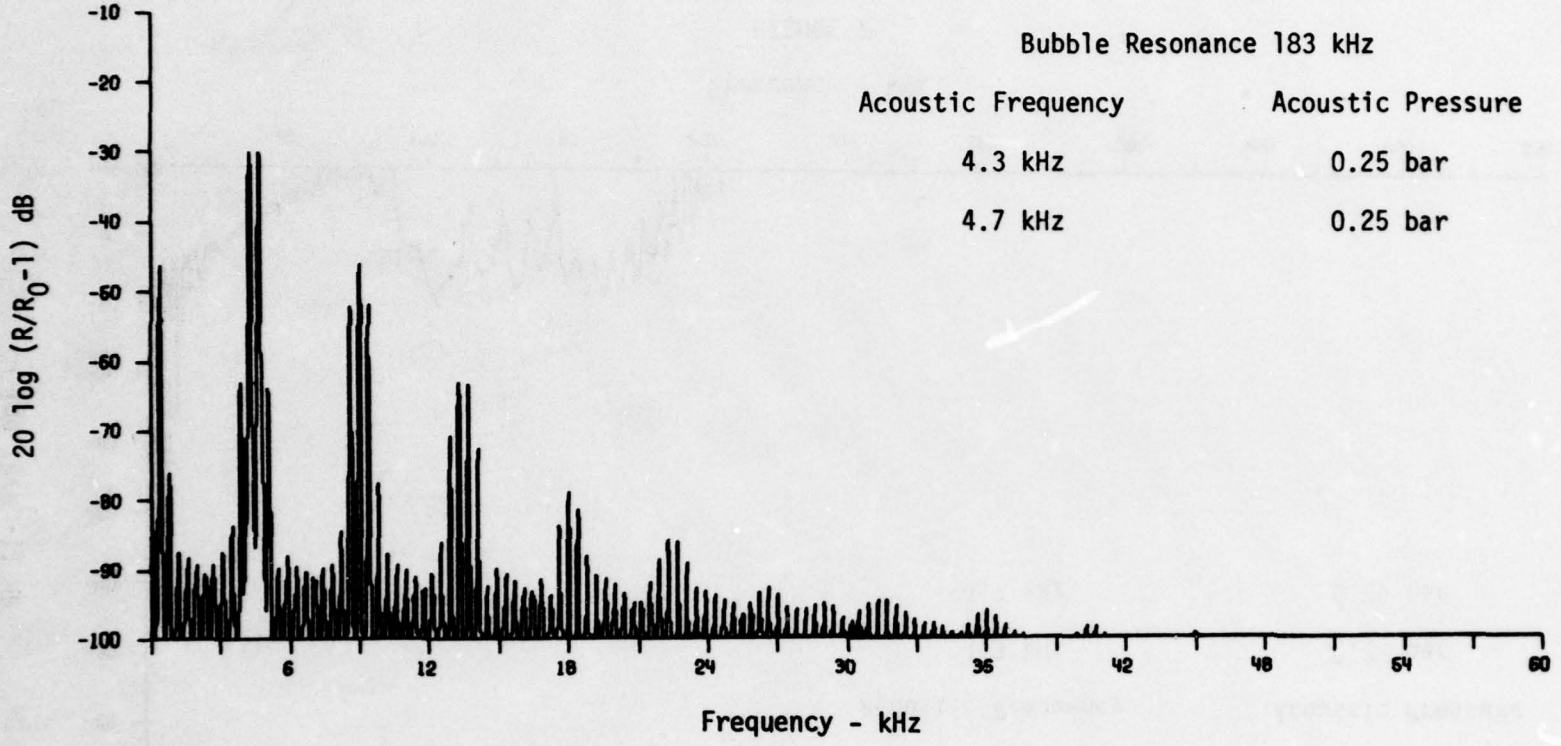

FIGURE 6

RADIAL MOTION SPECTRUM OF 20 μm BUBBLE

AS-78-1381
JRC 1095

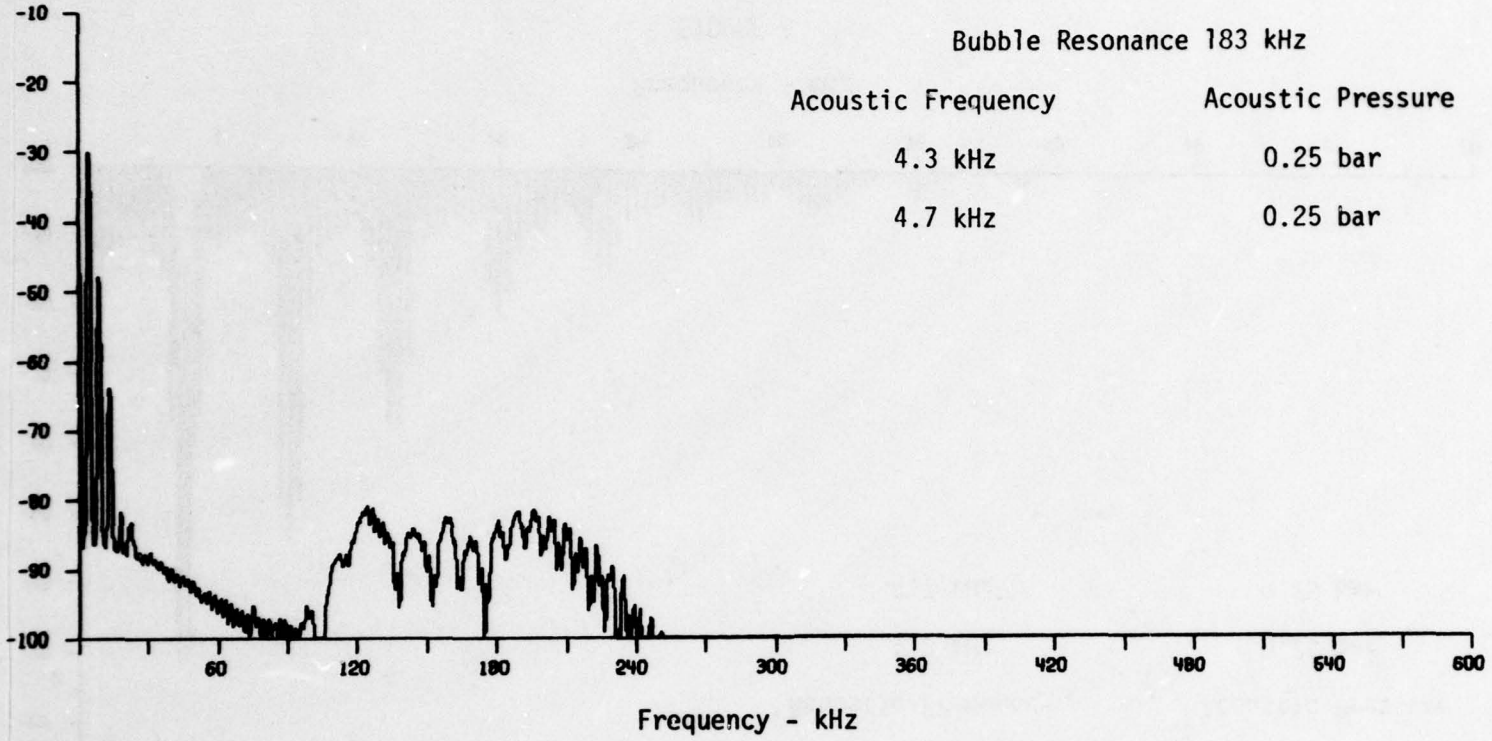

FIGURE 7

RADIAL MOTION SPECTRUM OF 20 μm BUBBLE

AS-78-1382
JRC 1095

including the region of the bubble resonance. In this case a band of energy about the natural resonance frequency exists, but no narrow line is present. The first peak in this band is at 106 kHz while the last peak at the same power level is at 223 kHz. This broadband feature is caused by the slow variation of the driving frequency pressure being seen as a variation in the ambient pressure by the 20 μm bubble whose resonance frequency is 183 kHz at 1 bar ambient pressure. This effect will be discussed later in section IV.D.

In Figs. 8 through 10 the spectrum of the 20 μm bubble driven at 0.5 bar per primary is shown. The number of lines is considerable, but all these "low frequency" lines are still sharp in Fig. 8. Figures 9 and 10 show that the lines form "beat groups", separated by 4.5 kHz, which finally merge into a general background level. This general background extends to well beyond the natural resonance frequency. Again the natural resonance has been spread by an effective variation in ambient pressure.

At even higher driving pressures the broadband energy from bubble collapses overwhelms all other effects and even the driving frequencies are masked. This is evident in Figs. 11 and 12, which show spectra of this bubble driven with 1.0 bar per primary signals. In Table II, the lines at f_1 and f_2 were at -16.7 dB at the 0.5 bar driving level. If increased by only 6 dB in going to 1.0 bar (as predicted by perturbation theory), they would be at -10 dB, which is 15 dB below the noise level in the vicinity of f_1 and f_2. The origin of the broad low frequency peaks around 550 Hz, 1100 Hz, 1200 Hz, etc., is unknown.

B. Medium Size Bubbles ($f_o > f_1, f_2$; $f_o < f_1 + f_2$)

To illustrate the intermediate case a 500 μm bubble driven with the same 4.3 kHz and 4.7 kHz driving frequencies was chosen. The natural resonance frequency of the 500 μm bubble is 7.13 kHz.

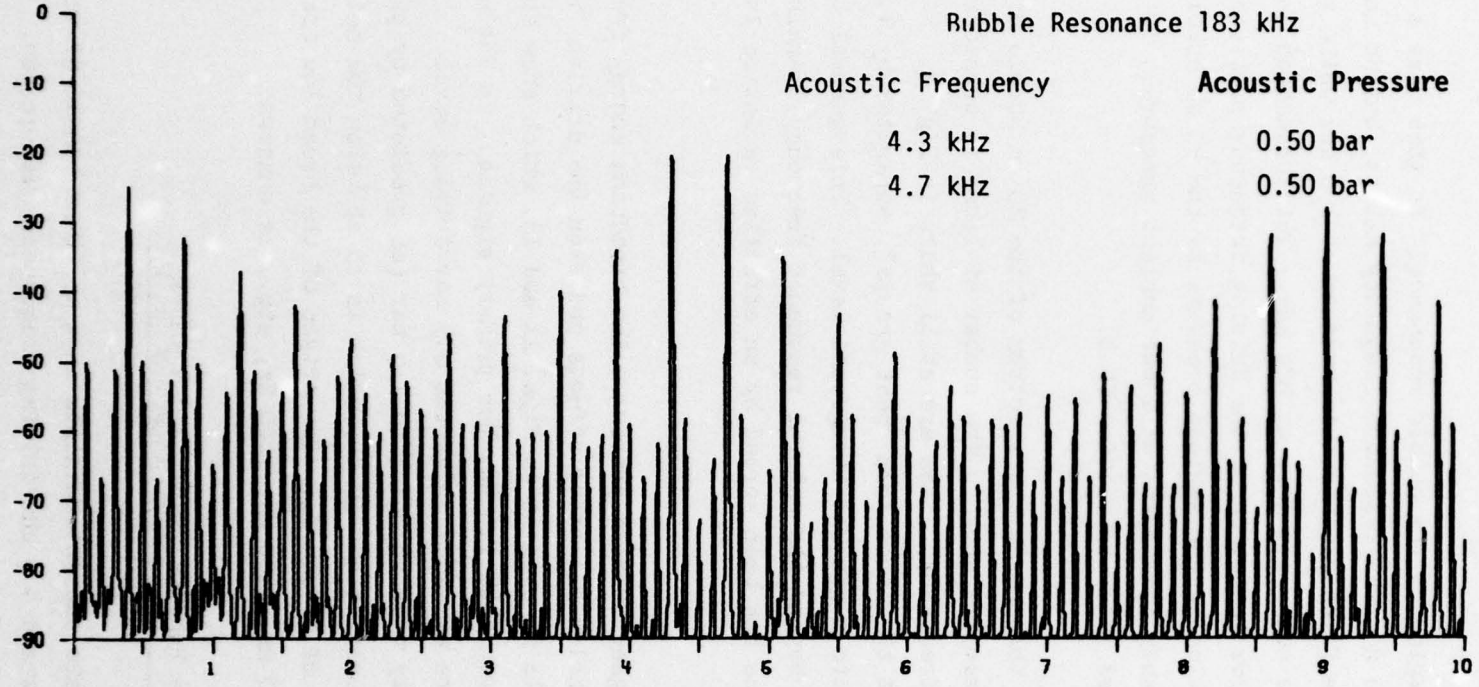

FIGURE 8

RADIAL MOTION SPECTRUM OF 20 μm BUBBLE

AS-78-1383
JRC 1095

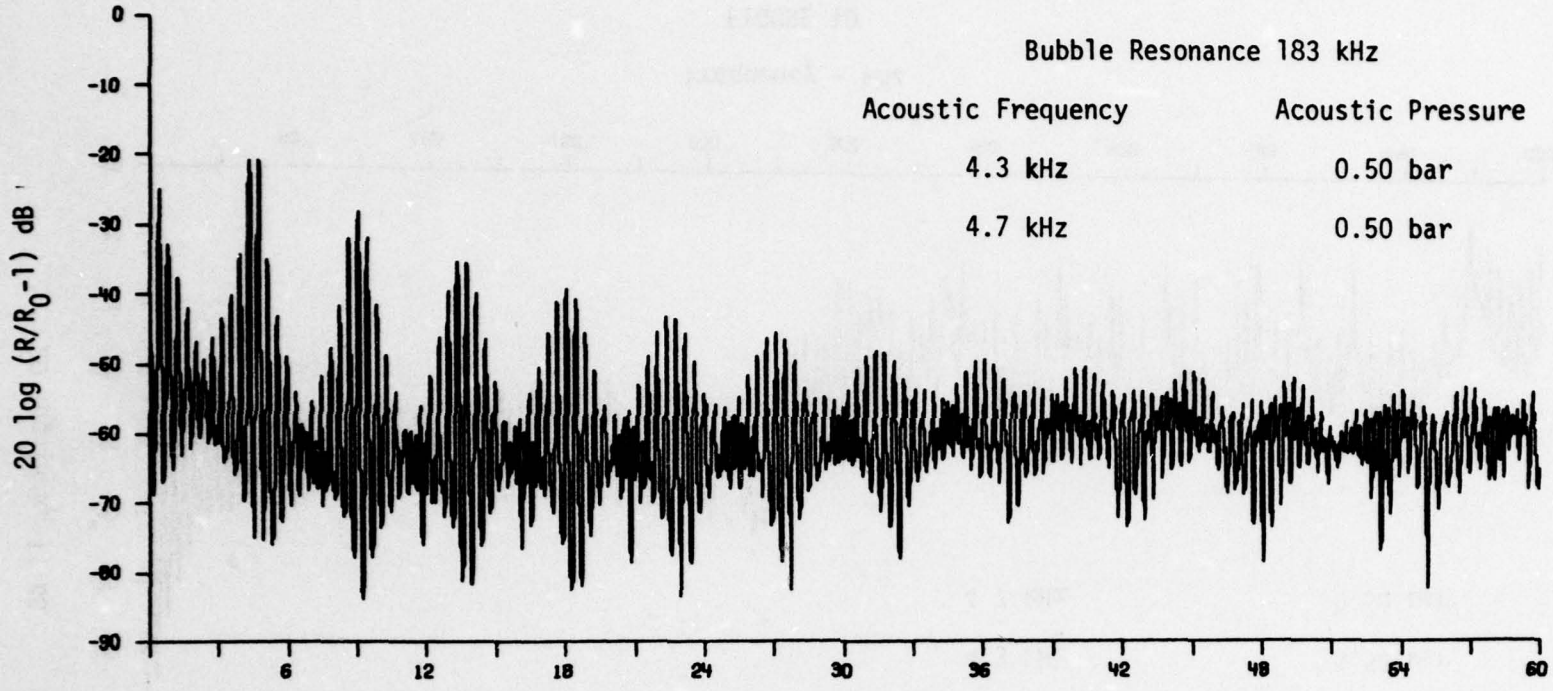

FIGURE 9

RADIAL MOTION SPECTRUM OF 20 μm BUBBLE

AS-78-1384
JRC 1095

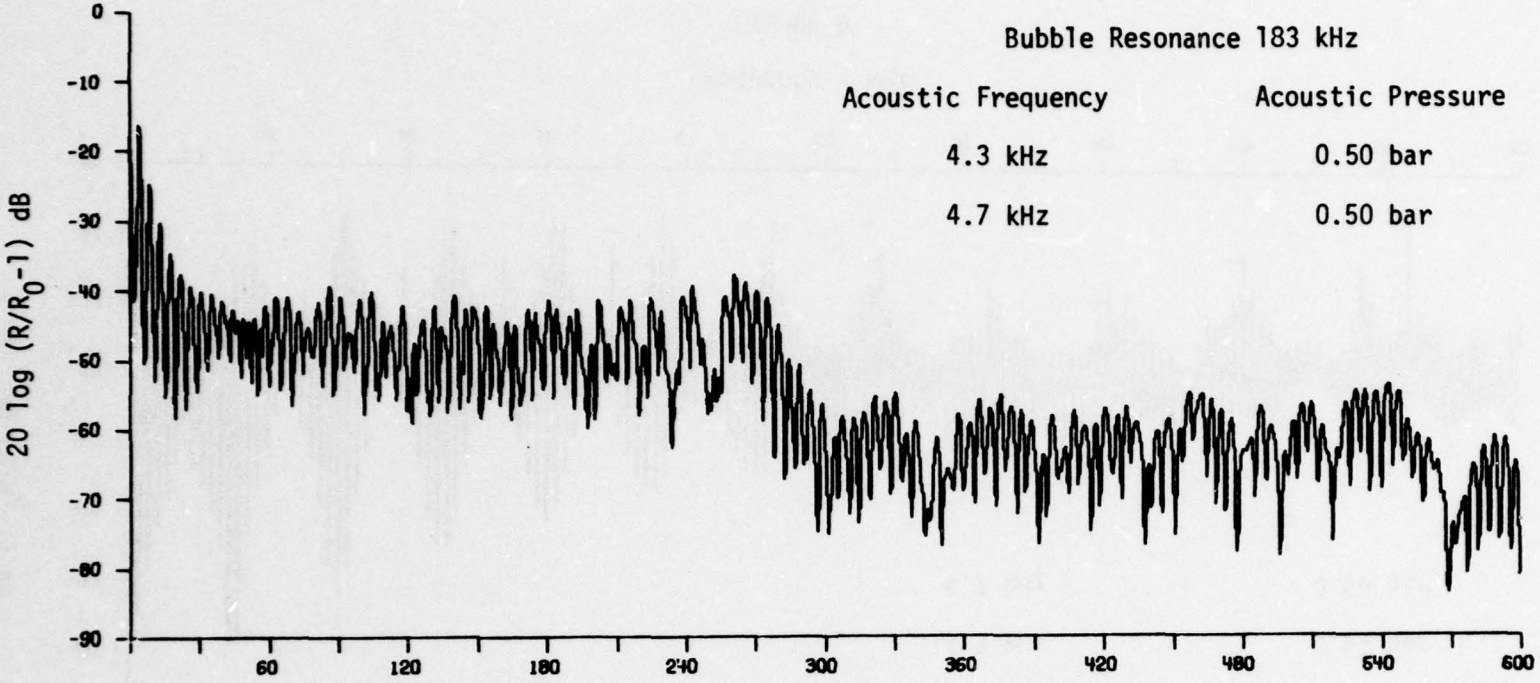

FIGURE 10

RADIAL MOTION SPECTRUM OF 20 μm BUBBLE

AS-78-1385
JRC 1095

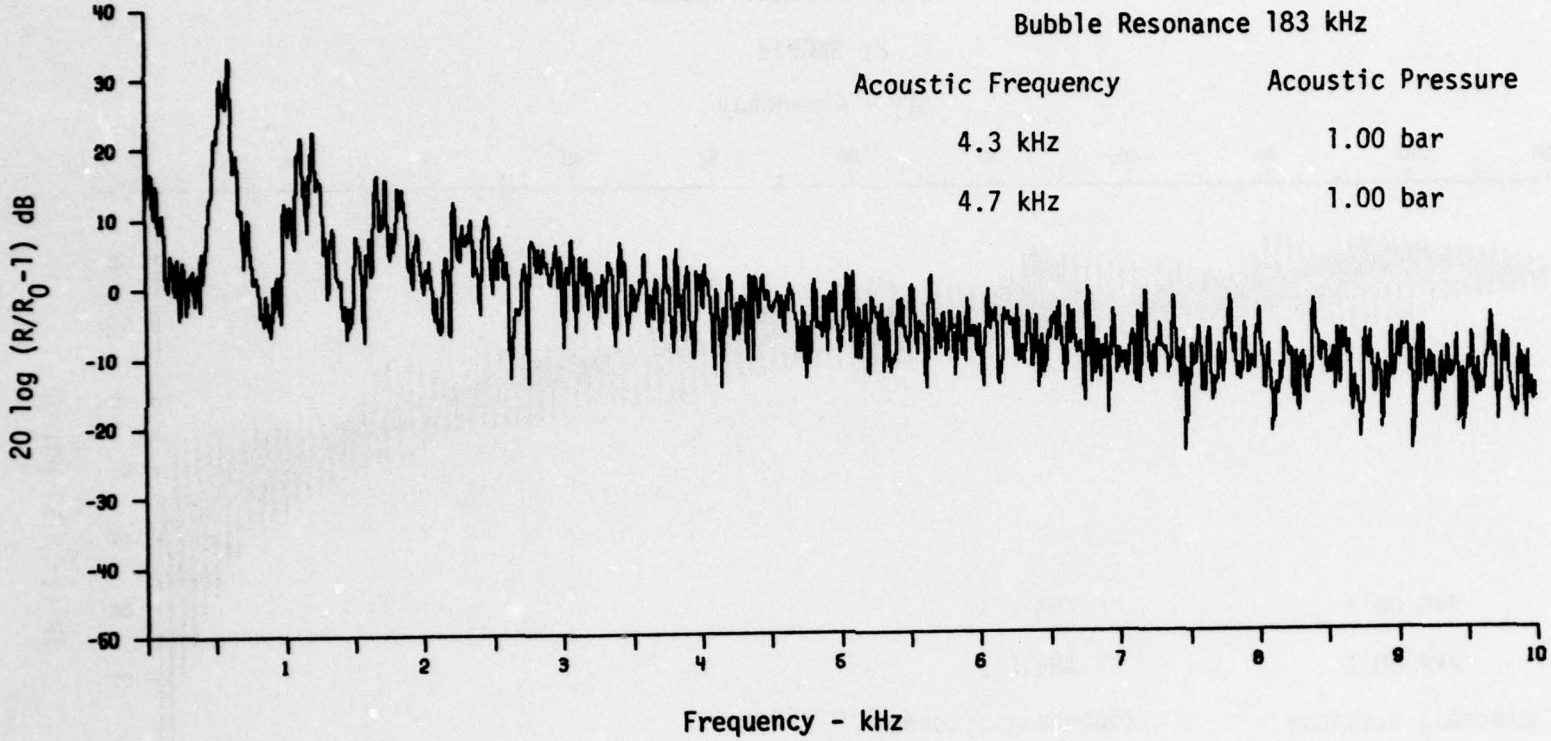

FIGURE 11

RADIAL MOTION SPECTRUM OF 20 μm BUBBLE

AS-78-1386
JRC 1095

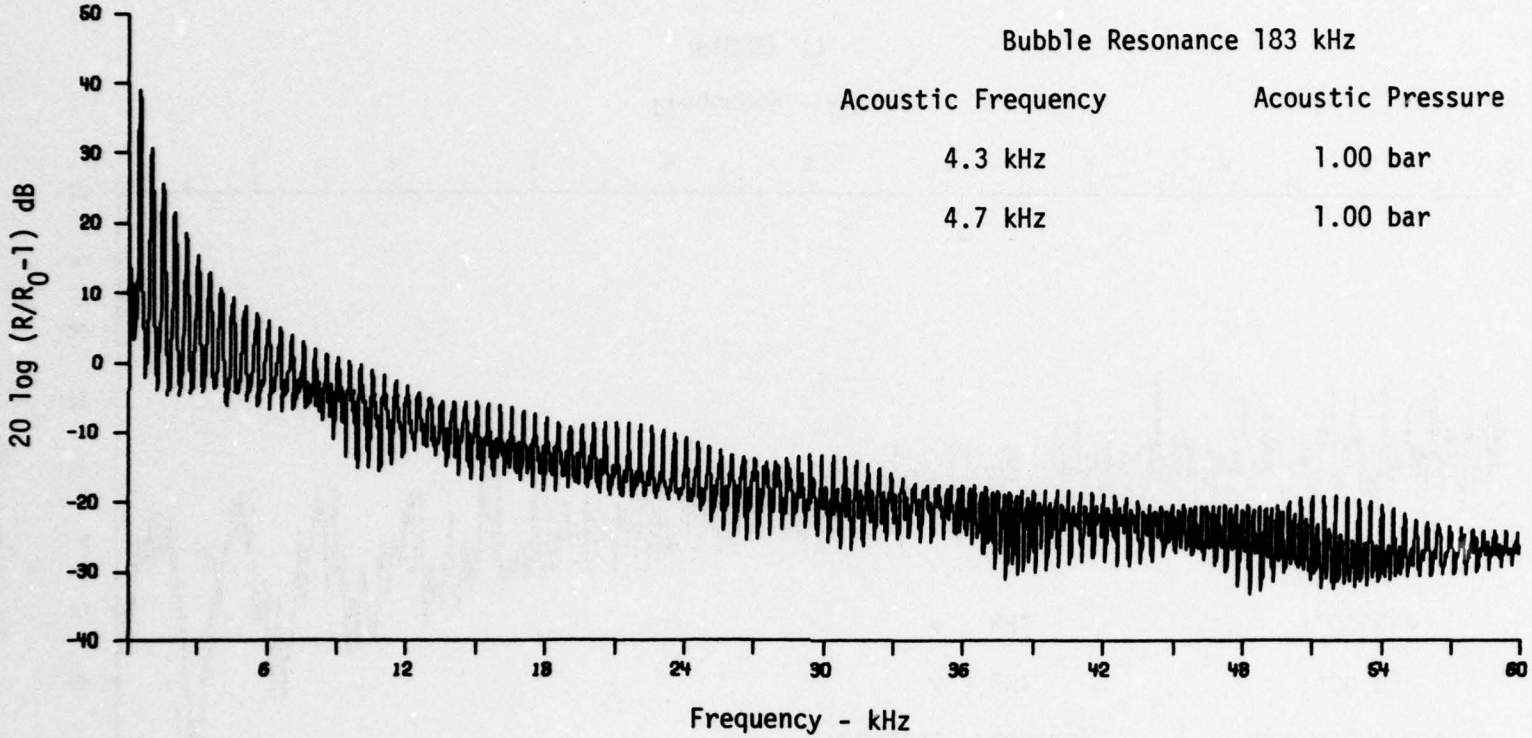

FIGURE 12

RADIAL MOTION SPECTRUM OF 20 μm BUBBLE

The spectrum of the bubble radial motion when the driving pressure is 0.1 bar per primary is shown in Fig. 13. In this case all lines are narrow, including the resonance line at 7.13 kHz. The third and higher order lines are also quite prominent even at this low driving pressure. Many of the frequency components on Fig. 13 have been labeled. The order of the term giving rise to the line is given in parentheses. Some fourth order lines show up on this graph.

Spectra for this case at driving pressures per primary of 0.25 bar, 0.50 bar, and 1.0 bar are shown in Figs. 14 through 16, respectively. At 0.25 bar, the general noise level is increasing, but many lines can still be distinguished. At 0.5 bar and 1.0 bar, all lines are masked by the general broadband noise. The dip formed by the noise decreasing from 0 Hz and the increased noise from the broadband (at 1.2 kHz on Fig. 14) was seen in many cases at high driving levels. An interesting feature of Fig. 16 is its similarity to Fig. 11. The absolute scales are also approximately the same when the normalization by R_o is removed. This implies that, at high driving pressures in the two-frequency case, the bubble spectrum becomes approximately independent of the original bubble size. The period between successive pressure absolute minimum, which is equal to the difference frequency period, apparently determines the maximum size to which the bubble can grow. If this explanation is correct, the spectra would not follow this pattern when f_2-f_1 approached the resonance frequency.

A summary of the line levels measurable in the 0.1 bar and 0.25 bar cases is shown in Table III. As with the small bubble case, perturbation theory predicted the 0.1 bar values quite well. The predictions for the first order terms also held true at 0.25 bar but the second order terms are in error by up to 5.7 dB.

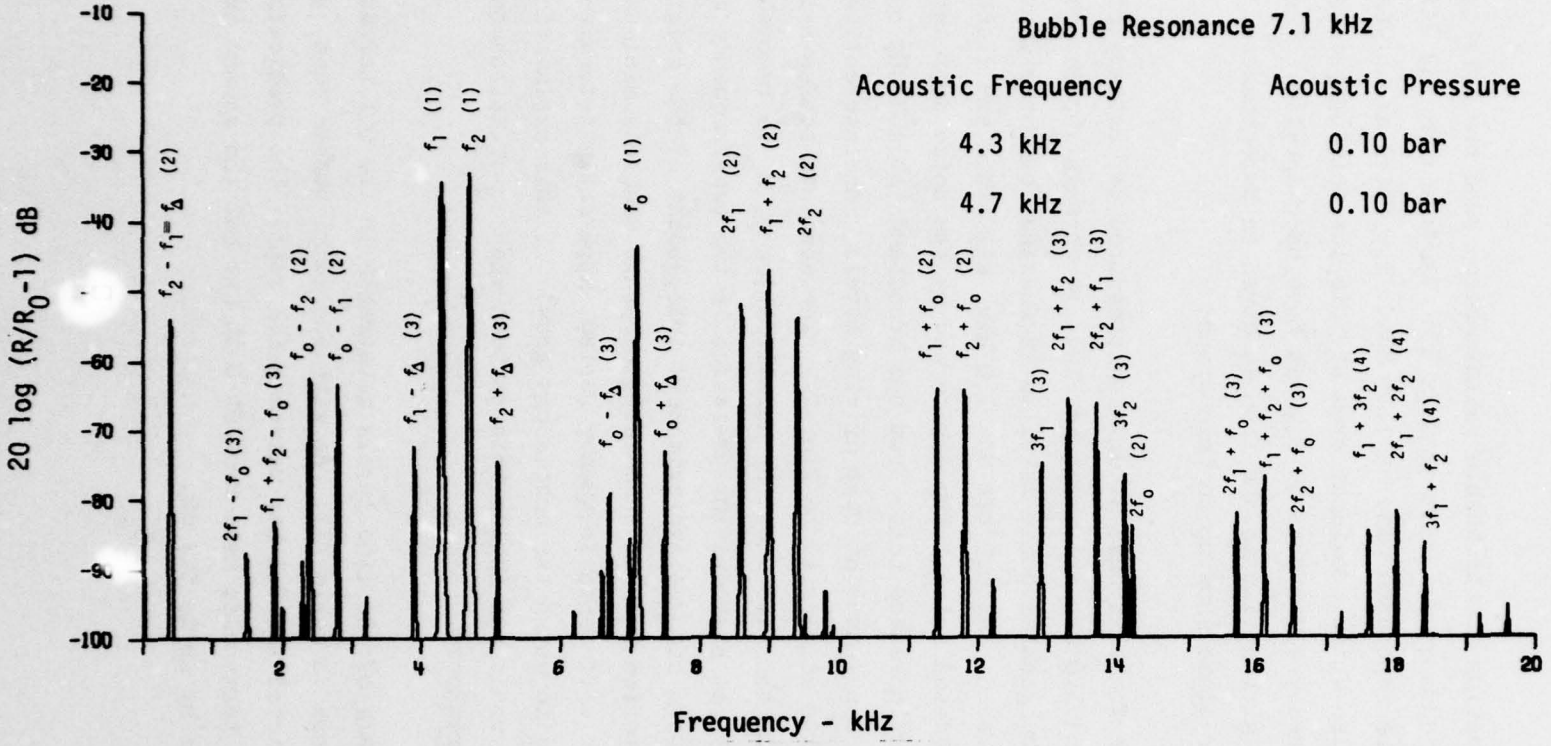

FIGURE 13

RADIAL MOTION SPECTRUM OF 500 μm BUBBLE

AS-78-1388
JRC 1095

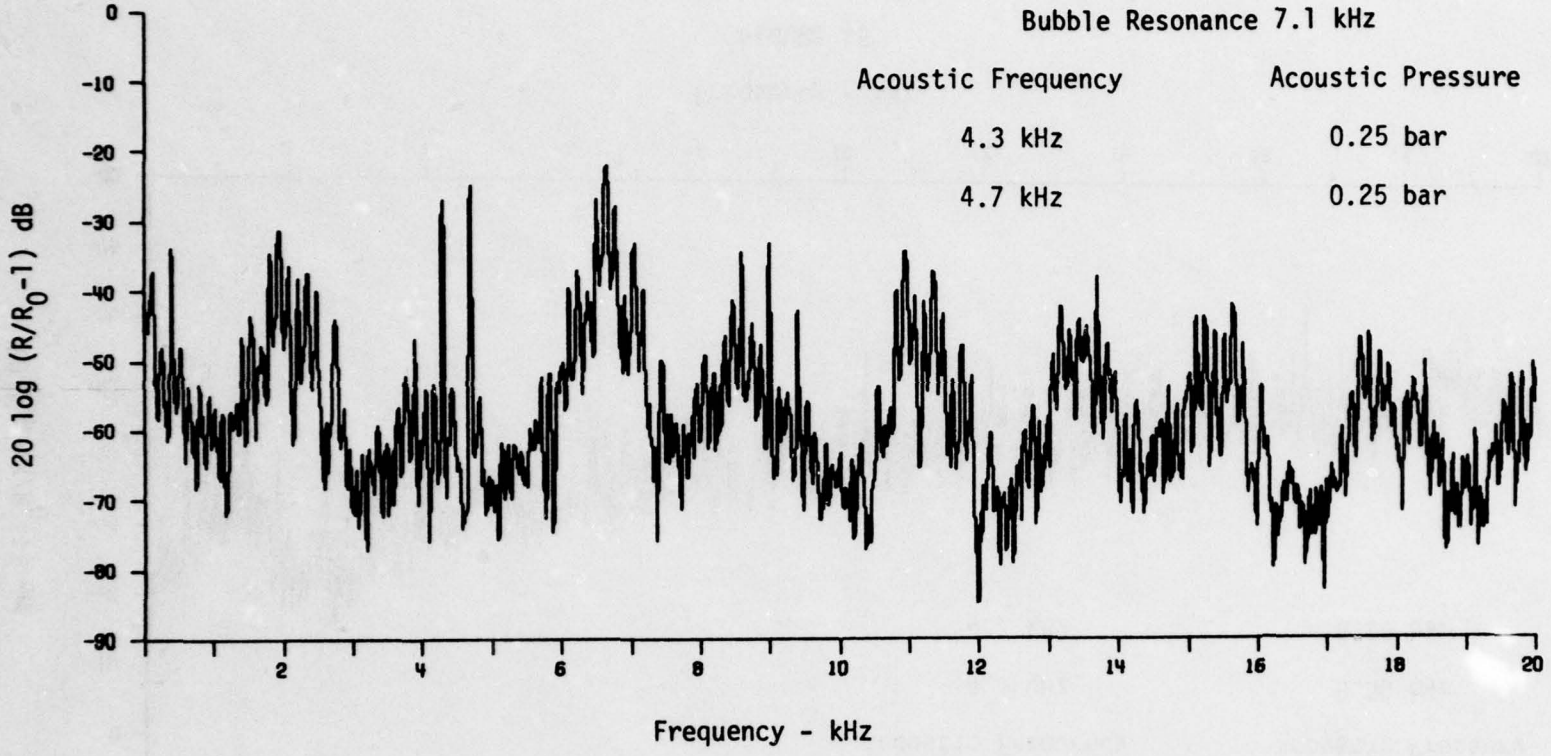

FIGURE 14

RADIAL MOTION SPECTRUM OF 500 μm BUBBLE

AS-78-1389
JRC 1095

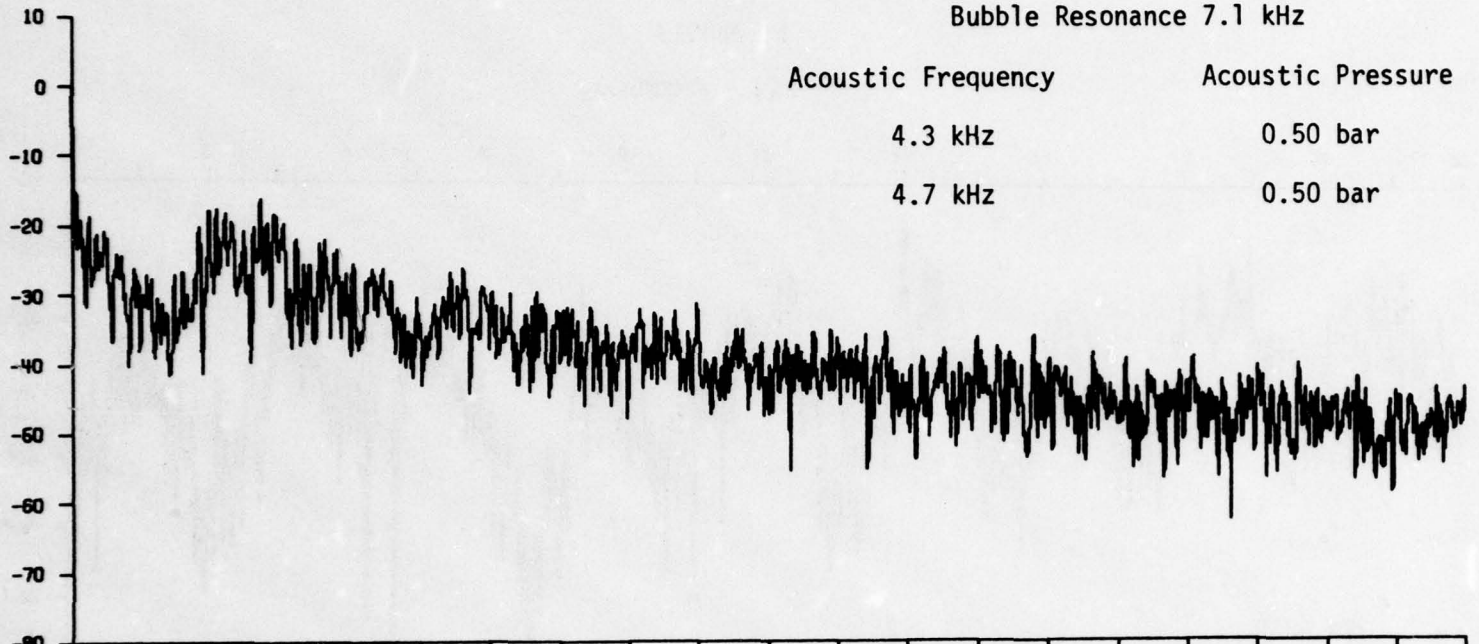

FIGURE 15

RADIAL MOTION SPECTRUM OF 500 μm BUBBLE

AS-78-1390
JRC 1095

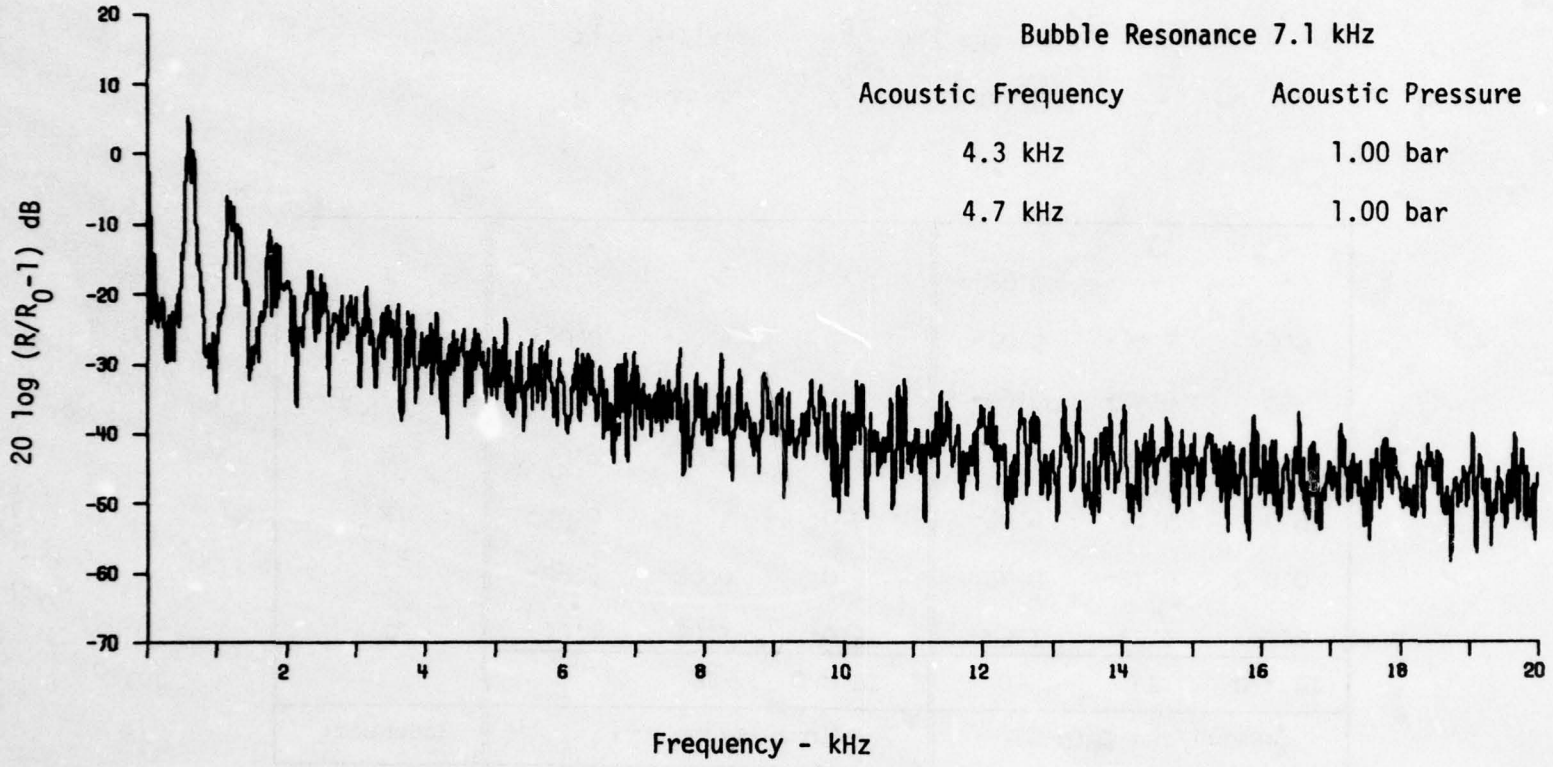

FIGURE 16

RADIAL MOTION SPECTRUM OF 500 μm BUBBLE

AS-78-1391
JRC 1095

TABLE III

NEAR-RESONANCE CASE
COMPARISON OF INTEGRATION RESULTS AND PERTURBATION THEORY

Values of x in decibels

Frequency	0.1 bar/primary			0.25 bar/primary		
	0	PT	0 - PT	0	PT	0 - PT
f_1	-30.4	-30.1	-0.3	-23.1	-22.1	-1.0
f_2	-29.3	-29.0	-0.3	-21.0	-21.0	0.0
$2f_1$	-48.0	-47.4	-0.6	-30.5	-31.4	0.9
$2f_2$	-49.7	-49.2	-0.5	-38.9	-33.2	5.7
$f_1 + f_2$	-42.9	-42.9	0.0	-29.3	-26.9	2.4
$f_2 - f_1$	-50.0	-50.1	0.1	-30.6	-34.1	-3.5
f_o	-39.5	-	-	-29.6	-	-

R_o = 500 μm f_o = 7.13 kHz

f_1 = 4.3 kHz f_2 = 4.7 kHz

0 = Integrated Results
PT = Perturbation Theory

C. Large Bubbles ($f_o < f_1, f_2$)

The large bubble regime was investigated using the same 500 μm bubble described in section IV.B. with driving frequencies of 15.8 kHz and 16.2 kHz. The difference frequency is therefore the same as in the two previous sections.

Figure 17 shows the radial motion spectrum of the 500 μm bubble. The same features shown for the medium bubble size in Fig. 13 are apparent in Fig. 17. The first and second order lines are narrow at the levels predicted by perturbation theory, as shown in Table IV.

The spectra of the same bubble driven with frequencies of 15.8 kHz and 16.2 kHz at pressures of 0.25 bar, 0.50 bar, 1.0 bar, and 1.5 bar are shown in Figs. 18 through 21, respectively. The levels of the lines can be followed to the 1.0 bar driving pressure level and are given in Table IV. Only at the 1.5 bar level does the broadband spectrum emerge, and even then, the driving frequencies and resonance frequency lines are evident.

The perturbation theory values are in good agreement through driving pressures of 0.5 bar/primary with the exception of the f_1+f_2 line, which is 1.5 dB high even at 0.1 bar, and the difference frequency line, which is beginning to grow rapidly at this level. One very positive result is that the difference frequency line is much larger than perturbation theory predicts. At 1.0 bar it is about 20 dB higher than expected. Although its precise value was not computed by the program, the 400 Hz line is still evident above the noise in Fig. 21 and probably has a value around -23 dB.

D. Effective Resonance Frequency

In several of the previous figures (Fig. 7 for example) the resonance was spread out. This occurred when the resonance frequency was higher

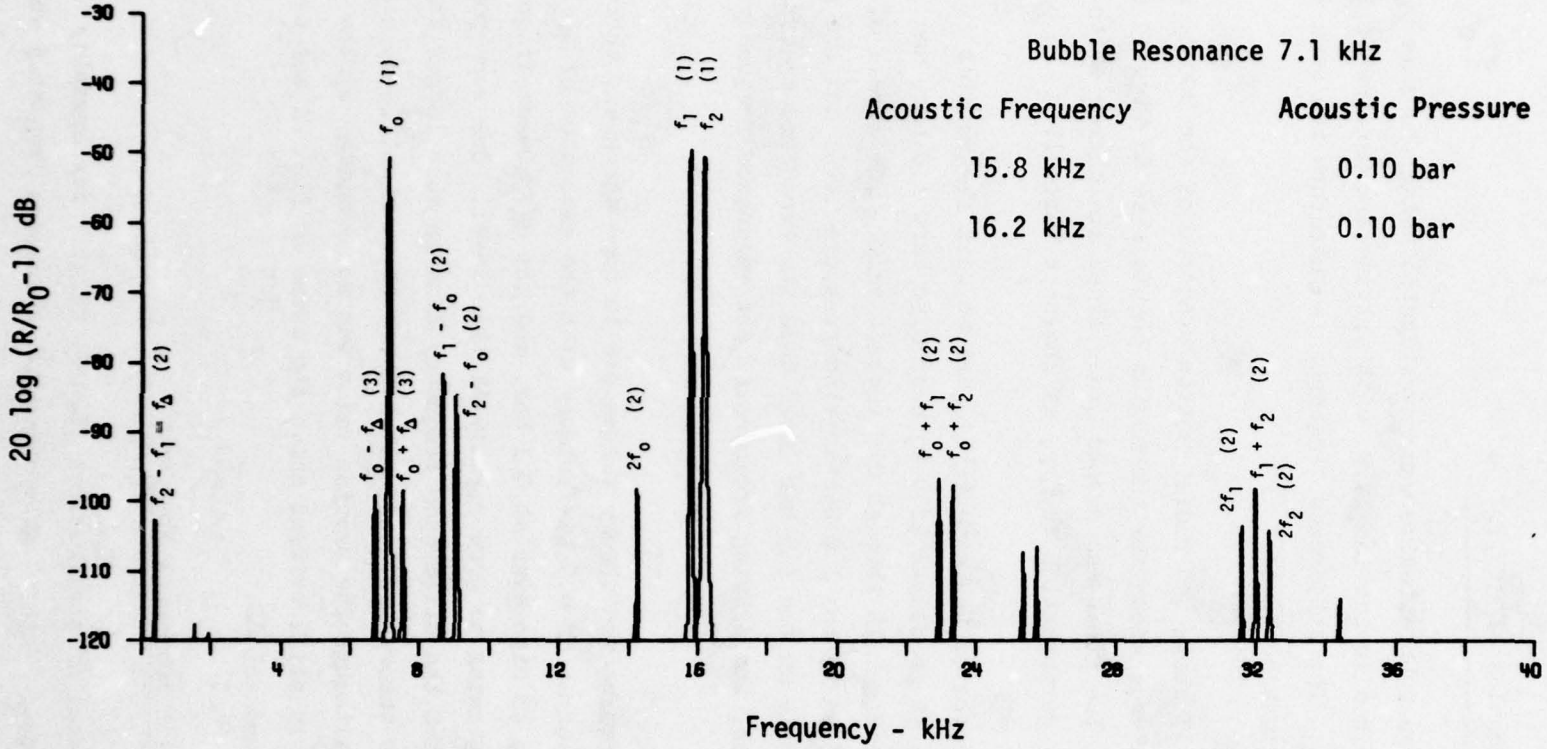

FIGURE 17

RADIAL MOTION SPECTRUM OF 500 μm BUBBLE

AS-78-1392
JRC 1095

TABLE IV

LARGE BUBBLE CASE

COMPARISON OF INTEGRATION RESULTS AND PERTURBATION THEORY

Values of x in decibels

P	0.1 bar/primary			0.25 bar/primary			0.5 bar/primary			1.0 bar/primary		
Frequency	0	PT	0 - PT	0	PT	0 - PT	0	PT	0 - PT	0	PT	0 - PT
f_1	-45.9	-45.8	-0.1	-37.9	-37.9	-0.1	-31.8	-31.8	0.0	-25.0	-25.8	0.8
f_2	-46.4	-46.4	0.0	-38.4	-38.4	0.0	-32.4	-32.4	0.0	-25.8	-26.4	0.6
$2f_1$	-99.5	-99.4	-0.1	-83.6	-83.4	-0.2	-71.4	-71.4	0.2	-53.6	-59.4	2.8
$2f_2$	-100.5	-100.6	-0.1	-84.7	-84.6	-0.1	-72.5	-72.6	0.1	-56.2	-60.6	4.4
$f_1 + f_2$	-94.0	-95.5	1.5	-78.1	-79.5	1.4	-65.9	-67.5	1.6	-49.9	-55.5	5.6
$f_2 - f_1$	-98.3	-98.5	0.2	-81.9	-82.5	0.4	-67.0	-70.5	3.5	-36.8	-58.5	21.7
f_o	-46.9	-	-	-38.6	-	-	-31.6	-	-	-20.2	-	-

R_o = 500 μm f_o = 7.13 kHz

f_1 = 15.8 kHz f_2 = 16.2 kHz

0 = Integrated Results

PT = Perturbation Theory

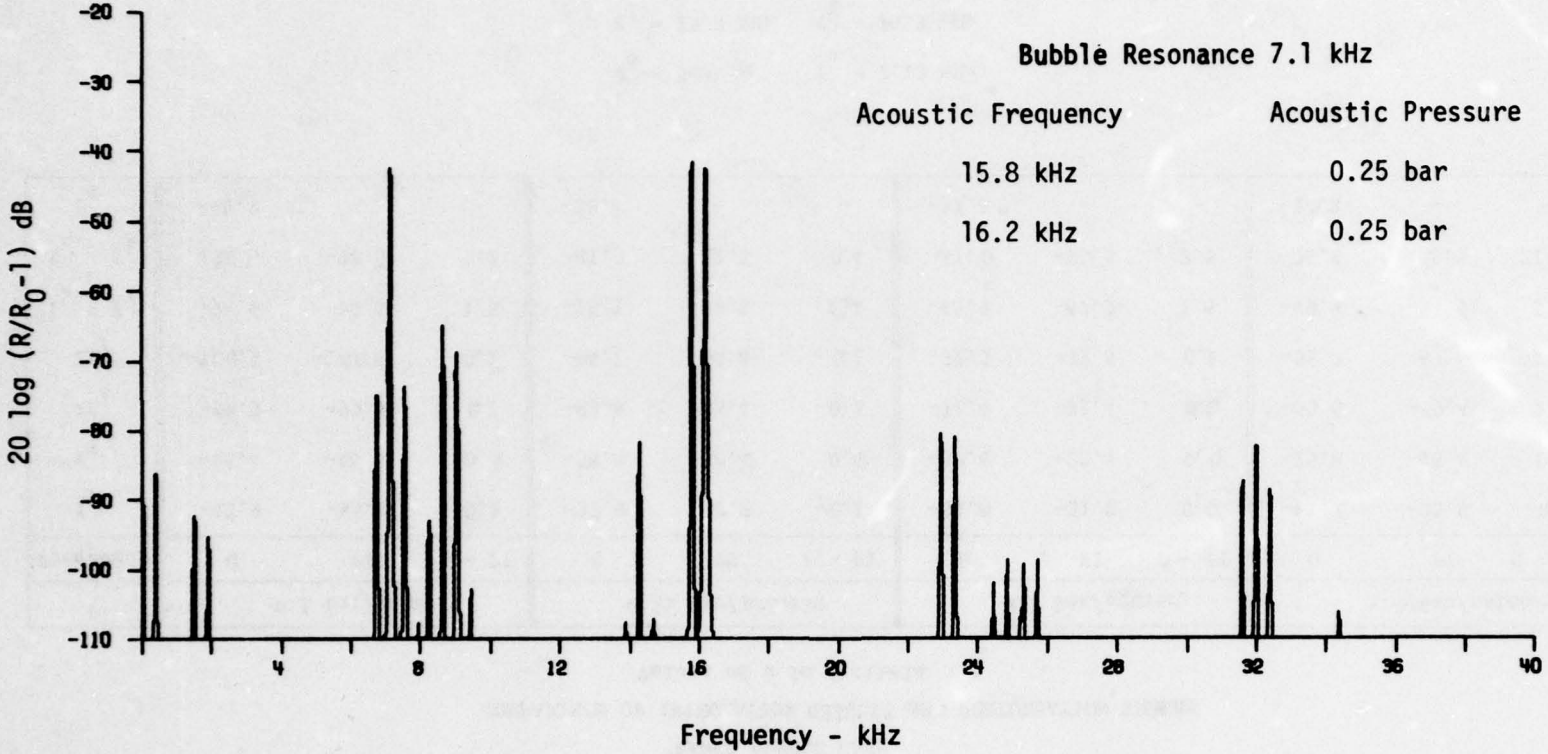

FIGURE 18

RADIAL MOTION SPECTRUM OF 500 μm BUBBLE

AS-78-1393
JRC 1095

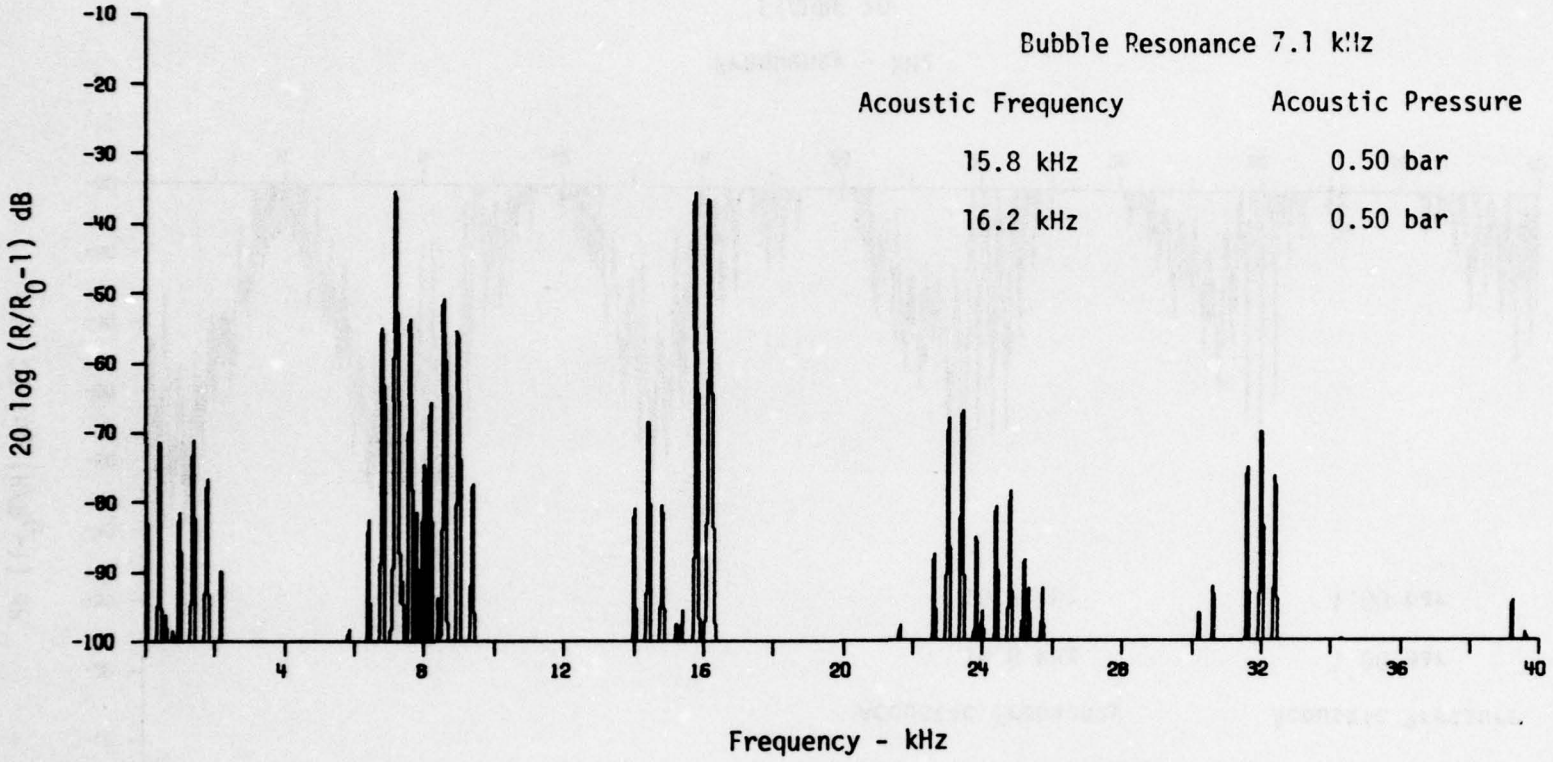

FIGURE 19

RADIAL MOTION SPECTRUM OF 500 μm BUBBLE

AS-78-1394
JRC 1095

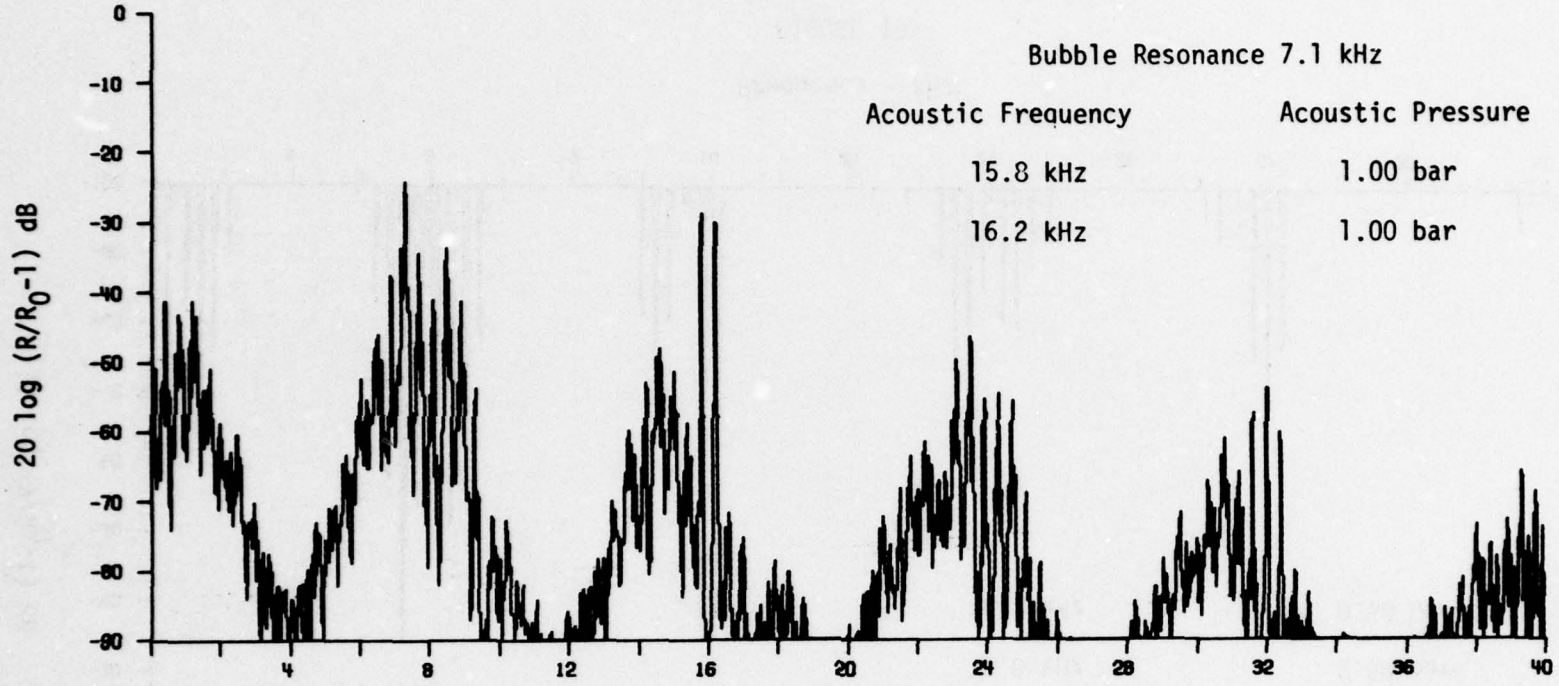

FIGURE 20

RADIAL MOTION SPECTRUM OF 500 μm BUBBLE

AS-78-1395
JRC 1095

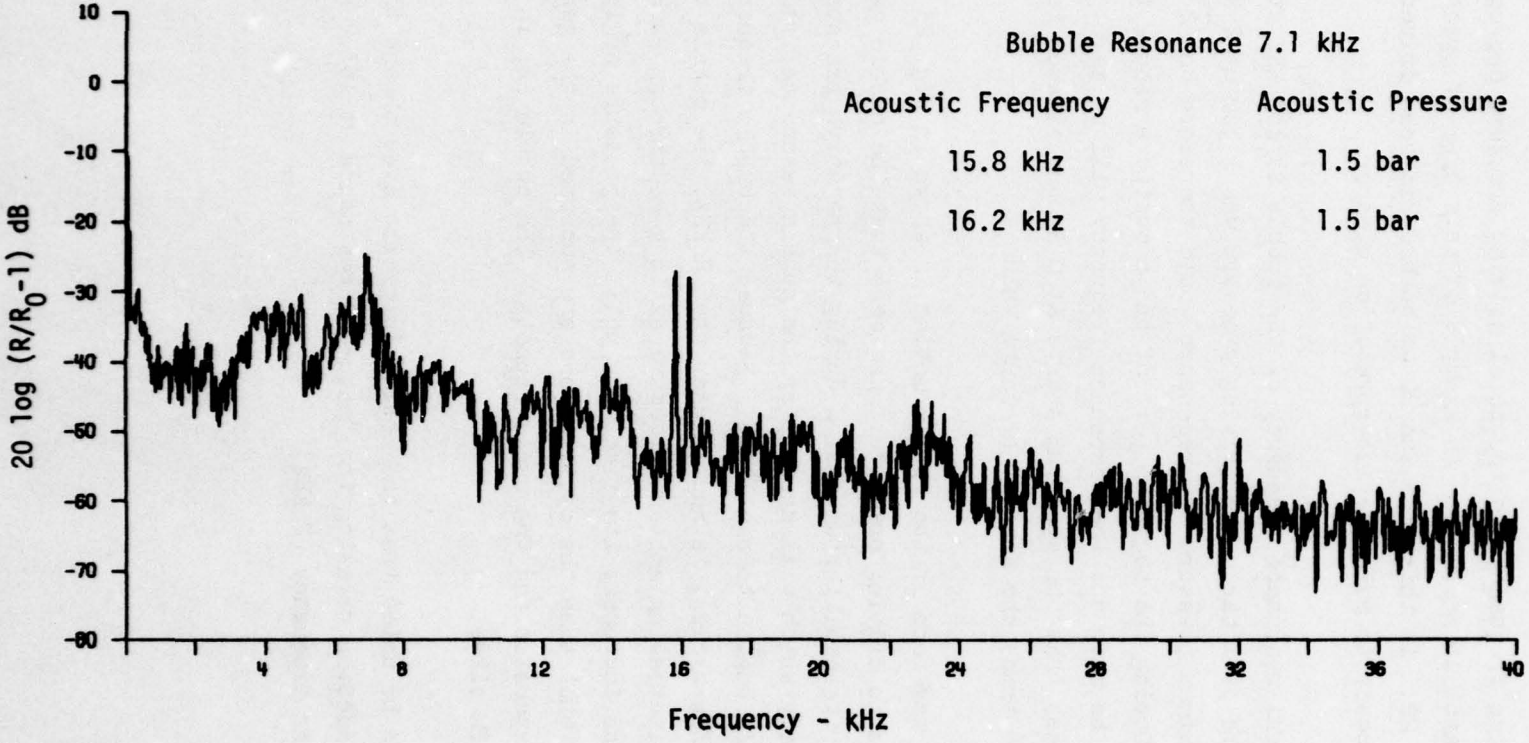

FIGURE 21

RADIAL MOTION SPECTRUM OF 500 μm BUBBLE

AS-78-1396
JRC 1095

than the driving frequency and the total driving pressure approached or exceeded the ambient pressure. An example of this type of spectrum is shown in Fig. 22. In this case the 20 μm bubble had been driven with only one frequency to make the interpretation clearer.

The natural resonance frequency of the bubble is 183 kHz at a static pressure of 1 bar. The driving pressure was 1 bar at 2 kHz. During the maximum pressure the resonance would therefore be $\sqrt{2} \times 183$ kHz or 259 kHz. During the negative part of the acoustic pressure the total pressure will be zero and the resonance frequency will be zero. In Fig. 22 one sees that the spectrum starts at 0 Hz but extends to about 290 kHz or 1.6 times the ambient pressure value.

The time waveform of the bubble motion is shown in Fig. 23 along with the acoustic driving pressure. One sees that the bubble expands to many times its equilibrium radius during the negative pressure phase, acquiring energy which will show up at the bubble resonance frequency once the bubble begins to oscillate. Because the bubble frequency, even on the first few cycles, is much higher than 2 kHz, the bubble experiences a constantly increasing ambient pressure as it goes through each oscillation and increases its frequency until the pressure begins to decrease. At that time the oscillations are subsumed in the general bubble oscillation expansion and the cycle repeats. The bubble is, in effect, executing an FM slide.

It should be noted that the motion is cyclic even though there is no rational fraction relating the "natural" resonance at 183.2 kHz and the driving frequency (2 kHz).

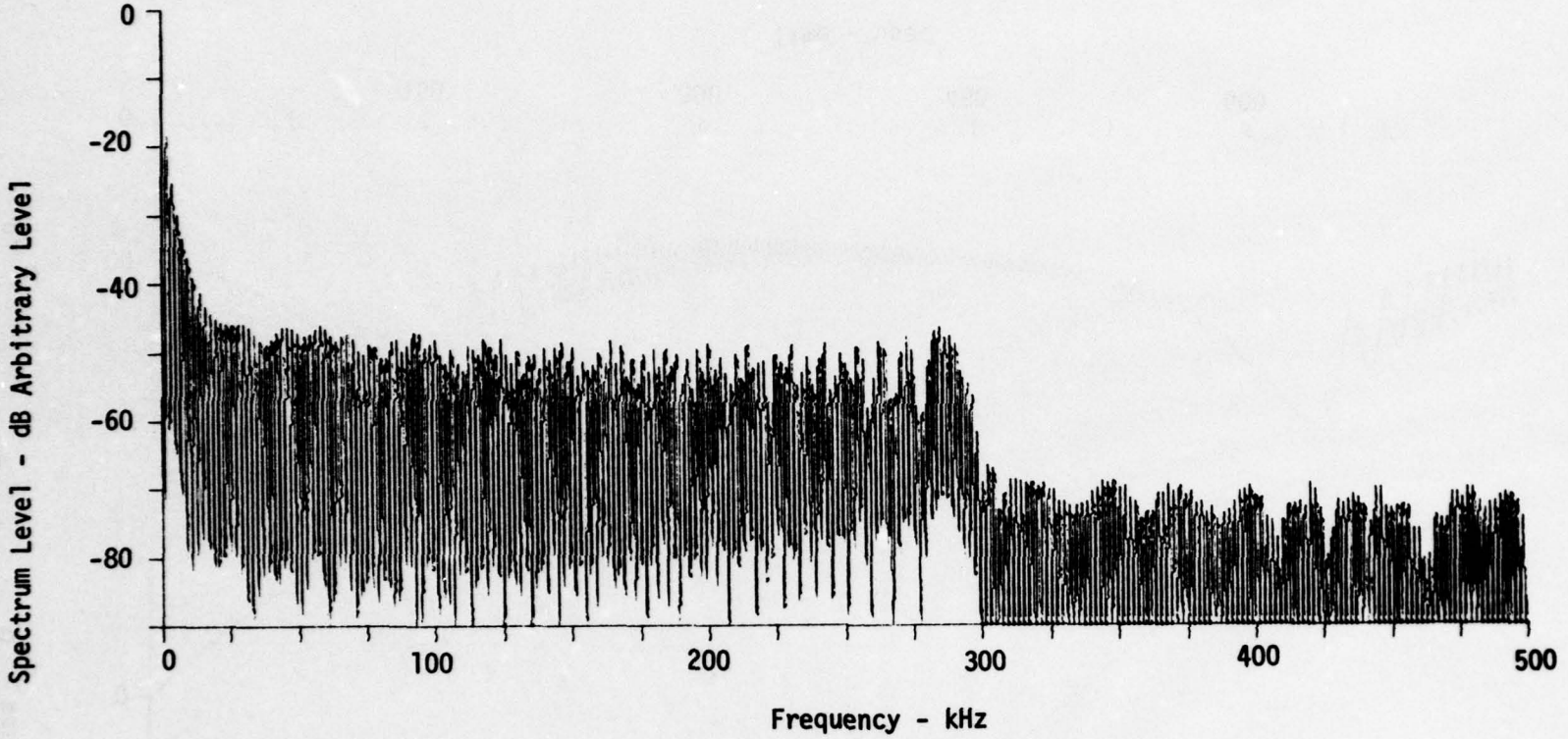

FIGURE 22

SPECTRUM OF RADIAL MOTIONS OF 20 μm BUBBLE UNDERGOING FM SLIDE

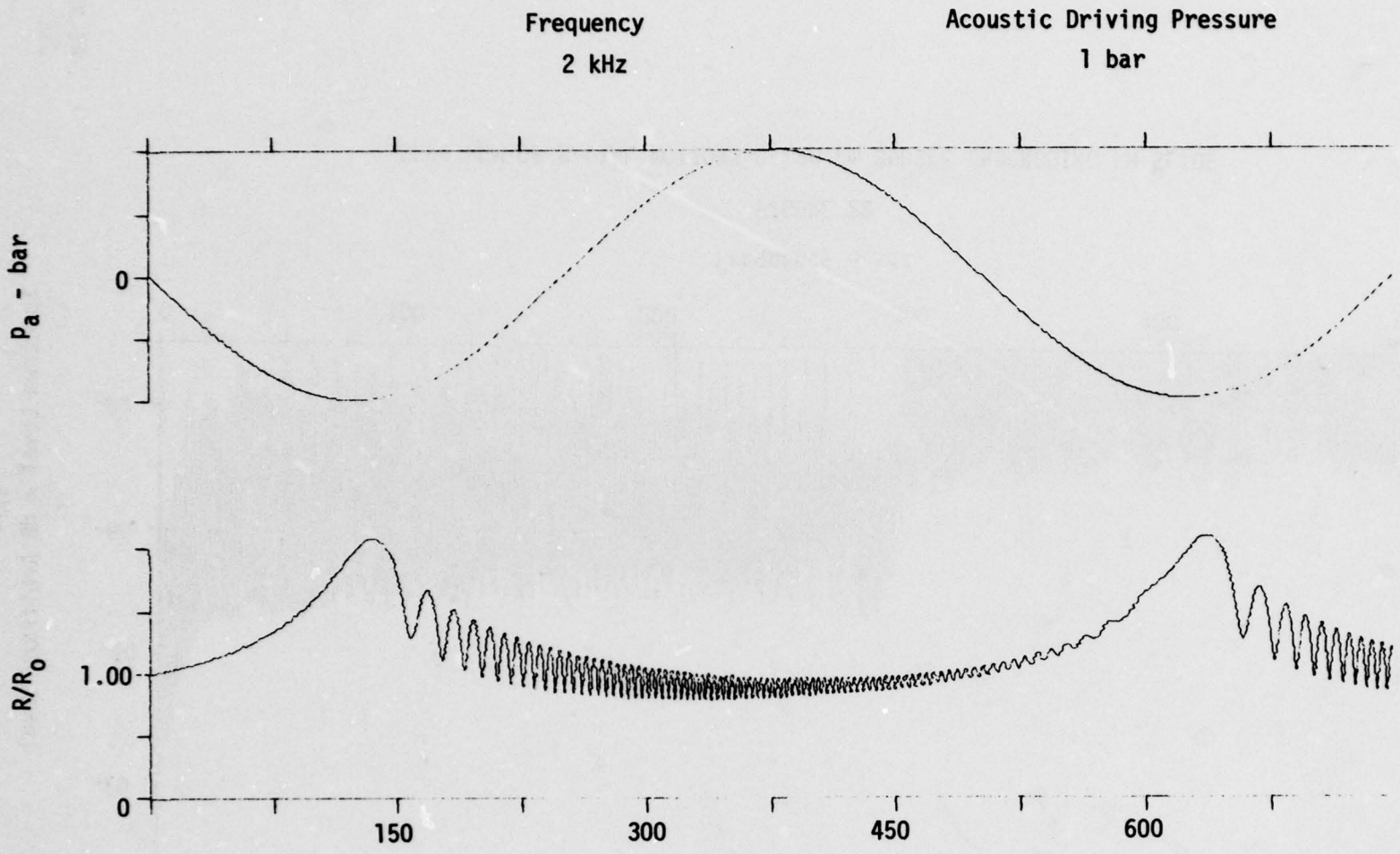

FIGURE 23

EXPANDED VIEW OF 20 μm BUBBLE UNDERGOING FM SLIDE OSCILLATIONS

AS-78-1398
JRC 1095

V. SUMMARY

The equation of motion of a gas bubble in water has been numerically integrated for the case of being driven by two intense acoustic waves at frequencies f_1 and f_2. Emphasis has been on the secondary frequency components generated by the nonlinear motion of the bubble, particularly the difference frequency f_2-f_1. Three cases have been examined in detail: driving frequencies far below resonance (small bubble), driving frequencies near resonance, and driving frequencies above resonance (large bubble).

The numerical results were compared to results obtained by perturbation theory. Agreement was excellent at driving pressures up to one quarter of the ambient pressure in the small bubble case, while the near-resonance results had already begun to diverge at this level. The large bubble results were in good agreement with perturbation theory at half-ambient driving pressures except for the difference frequency component, which was 3.5 dB larger than predicted.

In all cases, at medium pressures a myriad of sharp lines were present, sometimes resulting from fourth order interactions. At high driving pressures (equal to or greater than ambient) sharp bubble collapses created broadband noise which obliterated the sharp lines. This indicates that driving pressures below the cavitation level may be more useful in generating difference frequency sound.

The rather large enhancement of difference frequency level over the perturbation theory solution in the large bubble case indicates that large bubbles are probably more useful than small ones. In addition the lines are present to much higher driving pressure levels. In designing

experiments and equipment the problem of scattering, which increases as the fourth power of the radius, must be considered and a detailed trade-off study would be required.

ACKNOWLEDGMENTS

The authors express their thanks to Werner Lauterborn who supplied an early version of the computer program. The version was designated GASBUBL and had extensively been modified by the time GASBUBL5 was operational. All errors are therefore the responsibility of the authors.

APPENDIX

MAGNETIC TAPE FORMATS

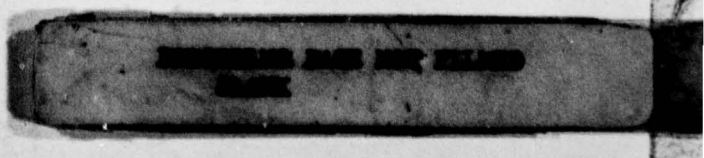

A. GASBUBL5 Output

GASBUBL5 outputs four multiplexed channels of data to magnetic tape in SPIO format.* These channels are time (T), bubble radius (R), bubble wall velocity ($\dot{R}$), and bubble wall acceleration ($\ddot{R}$) in that order. The data are grouped in units of 2048 points per array. Each of these units is called a "sequence" and consists of two physical records: an identification record (IDR) and a data record (DR). The IDR's are 121 CDC 3200 integer words long and the DR's are 8096 (4*2048) CDC 3200 integer words long. The records were written with BUFFER OUT in odd parity at 800 bpi. Each sequence takes 3.6 ft of tape allowing about 640 sequences to be placed on a 2400 ft tape.

Each IDR contains coded information to allow easy I/O using routines available at ARL:UT and information about the parameters used in the integration. Each IDR is equivalenced in GASBUBL5 to an integer (ID) and a floating point (XD) array. Because it requires two 24-bit CDC 3200 words to store one 48-bit floating point word, XD is only 60 elements long. The storage format of the IDR is given in Table AI.

The four multiplexed data channels have been scaled and stored as 24-bit integers prior to being placed on magnetic tape. The scale factors and other quantities necessary to retrieve the true values of the data are stored in the IDR. Because of automatic scaling within GASBUBL5, these scale factors may not be the same from sequence to sequence. To recover the data on a CDC 3200 computer, one must input the IDR and set

RZERO = XD(32),
SCLT = XD(42),
SLCR = XD(43),
SCLRD = XD(44), and
SCLRDD = XD(45).

*A detailed explanation of this format is given in Ref. 18. However, the information in this appendix should be sufficient for a programmer to be able to read the tapes.

TABLE AI

GASBUBL5 IDENTIFICATION RECORD

Integer Array

ID Index	Storage Usage
1	Number of elements in each array in following DR (2048).*
2	Sequence number, a sequential record index.
11	Initial suggested sample frequency (kHz)
19,21	Used by I/O routines.
91	Number of steps to back up in major restart (20).
93	Number of this sequence within current integration. If negative, indicates last sequence in integration.
94	Maximum number of consecutive step size reductions before doing a major restart (1).
100	Number of arrays multiplexed in DR (4).
121	Characters "SPIT", used to locate ID records.

Floating Point Array

XD Index		Storage Usage
22	γ	Adiabatic exponent
23	σ	Surface tension (dynes/cm)
24	P_o	Ambient pressure (bars)
25	μ	Viscosity (poise)
26	ρ_o	Fluid density (g/cm^3)
27	f_1	First driving frequency (kHz)
28	P_1	Amplitude of pressure at frequency f_1 (bars)
29	f_2	Second driving frequency (kHz)
30	P_2	Amplitude of pressure at frequency f_2 (bars)
31	φ	Beginning phase difference in driving amplitudes (radians)
32	R_o	Equilibrium radius (μm)
33	P_v	Vapor pressure inside bubble (bars)
34	t	Initial time for this integration (μsec)
35	R	Initial bubble radius for this integration (μm)
36	$\dot{R}$	Initial bubble wall velocity for this integration (μm/μsec=m/sec)

*Numbers in parentheses are default values.

TABLE AI (Cont'd)

XD Index	Storage Usage
37	Fractional part of period which step size will not exceed (0.01)
38	Factor by which time step increased and reduced in minor adjustments (2)
39	S_k Test factor on Runge-Kutta k's (0.03)
40	f_o Bubble resonance frequency (kHz)
41	C_o Sound speed, if zero, acoustic terms omitted from integration
42	SCT Scale factor for time array
43	SCR Scale factor for R array (this DR)
44	$SC\dot{R}$ Scale factor for $\dot{R}$ array (this DR)
45	$SC\ddot{R}$ Scale factor for $\ddot{R}$ array (this DR)
51	T(1) Beginning time in this DR (μsec)
52	R(1) Beginning radius in this DR (μm)
53	$\dot{R}$(1) Beginning bubble wall velocity in this DR (μm/μsec)
54	T(Last) Last time in this DR (μsec)
55	R(Last) Last radius in this DR (μm)
56	$\dot{R}$(Last) Last bubble wall velocity in this DR (μm/μsec)
57	Δt_{lim} Maximum allowed Δt (μsec)
58	Δt_{min} Minimum Δt, this DR (μsec)
59	Δt_{max} Maximum Δt, this DR (μsec)
60	Program name (Characters "GASBUBL5")

The DR can then be read into an integer array (IA) dimensioned (4,2048). The time in microseconds is given by

$$T(I) = IA(1,I) * SCLT \quad ,$$

the radius in micrometers by

$$R(I) = IA(2,I) * SCLR * RZERO \quad ,$$

$\dot{R}$ in micrometers per microseconds by,

$$RD(I) = IA(3,I) * SCLRD * RZERO \quad ,$$

and $\ddot{R}$ by

$$RDU(I) = IA(4,I) * SCLRDD * RZERO \quad .$$

B. Resampled Output

The program GASRSMPL accepts the output of GASBUBL5 and produces an output tape of R, $\dot{R}$, and $\ddot{R}$ array multiplexed as in GASBUBL5. The data are equally spaced in time as directed by control cards. The storage format is the same as that used by GASBUBL5 except that

(1) only three arrays are multiplexed (time is absent),
(2) ID(100) is 3,
(3) XD(60) is "GASRSMPL," and
(4) XD(42) to XD(59) have been changed to reflect the nature of the data stored on the following DR (e.g., XD(57), XD(58), and XD(59) are all set to the time step).

REFERENCES

1. H. G. Flynn, "Physics of Acoustic Cavitation in Liquids," Physical Acoustics, W. Mason (ed.) (Academic Press, New York, 1964), Vol IB, p. 58.

2. M. S. Plesset and A. Prosperetti, "Bubble Dynamics and Cavitation" in Ann. Rev. Fluid Mech. 9, 145 (1977). This is a good recent review citing many references.

3. P. J. Westervelt, "Parametric Acoustic Array," J. Acoust. Soc. Am. 35, 535 (1963).

4. T. Muir and J. Blue, "Experiments in the Acoustic Modulation of Large-Amplitude Waves," J. Acoust. Soc. Am. 46, 227 (1969).

5. D. J. Dunn, M. Kuljis, and V. G. Welsby, "Nonlinear Effects in a Focused Underwater Standing Acoustic Wave System," J. Sound Vib. 2, 471 (1965).

6. V. G. Welsby and M. H. Safar, "Acoustic Nonlinearity Due to Microbubbles in Water," Acustica 22, 177 (1969).

7. J. S. M. Rusby, "The Onset of Sound Wave Distortion and Cavitation in Water and Sea Water," J. Sound Vib. 13, 257 (1970).

8. W. L. Konrad and M. B. Moffett, "Difference Frequency Radiation from a Cavitating Parametric Source," J. Acoust. Soc. Am. 55, 42E(A). See also Naval Underwater Systems Center Technical Memorandum No. TDIX-45-73, 1973.

9. T. G. Muir, "Nonlinear Parametric Transduction in Underwater Acoustics," 1974 Ultrasonics Symposium Proceedings, IEEE Cat. No. 74, CHO 896-ISU.

10. J. Clynch and R. Rolleigh, "Measurement of Enhanced Nonlinear Radiation in the Presence of Microbubbles," J. Acoust. Soc. Am. 55S 51(A) (1974). Also, Applied Research Laboratories Technical Memorandum No. 74-17 (ARL-TM-74-17), Applied Research Laboratories, The University of Texas at Austin, May 1974.

11. J. Lockwood and D. Smith, "Investigation of the Increase in Parametric Efficiency Due to Bubbles," J. Acoust. Soc. Am. 57S, 73(A) (1975). Also AMETEK Technical Report, 11-1354E-74-1, 20 August 1974.

12. J. R. Clynch and C. W. Dittman, "Bubble Enhanced Nonlinear Sound Generations," J. Acoust. Soc. Am. 59S, 88(A), 1976.

13. M. B. Moffett and W. L. Konrad, "Experiments with Cavitating Parametric Sources," J. Acoust. Soc. Am. 60S, 99(A), 1976. See also Naval Underwater Systems Technical Memorandum TM-316-568-76, 1 December 1976.

14. H. G. Flynn, "Cavitation Dynamics, I. A Mathematical Formulation," J. Acoust. Soc. Am. 57, 1379 (1975).

15. H. G. Flynn, "Cavitation Dynamics II. Free Pulsations and Models for Cavitation Bubbles," J. Acoust. Soc. Am. 58, 1160 (1975).

16. W. Lauterborn, "Numerical Investigation of Nonlinear Oscillations of Gas Bubbles in Liquids," J. Acoust. Soc. Am. 59, 282 (1976).

17. D. Epstein, "Effect of a Dense Gas Equation on the Expansion and Contraction of an Underwater Gas Bubble," J. Acoust. Soc. Am. 57, 1427 (1975).

18. J. K. Vaughan, M. W. Ohlendorf, and R. L. Sweet, "An Input-Output Software System for Signal Processing," Applied Research Laboratories Technical Report No. 74-6 (ARL-TR-74-6), Applied Research Laboratories, The University of Texas at Austin, 20 May 1974.

12 September 1978

DISTRIBUTION LIST FOR
ARL-TR-78-40
UNDER CONTRACT N00014-76-C-1095
UNCLASSIFIED

Copy No.

Chief of Naval Research
Department of the Navy
Arlington, VA 22217
1 Attn: Physics Program Office (Code 421)
2 - 7 Code 102IP
8 Assistant Chief for Technology (Code 200)

Director
Defense Advanced Research Projects Agency
1400 Wilson Blvd.
Arlington, VA 22209
9 - 11 Attn: Technical Library

Director
Naval Research Laboratory
Department of the Navy
Washington, DC 20375
12 Attn: Technical Library
13 - 18 Code 2627

Office of the Under Secretary of Defense for
Research and Engineering
The Pentagon
Washington, DC 20301
19 - 21 Attn: Information Office Library Branch

22 - 23 U.S. Army Research Office
Box 12211
Research Triangle Park
North Carolina 27709

24 - 26 Commanding Officer
Department of the Navy
Office of Naval Research Branch Office
536 Clark Street
Chicago, IL 60605

27 - 29 Commanding Officer
Office of Naval Research Branch Office
1030 East Green Street
Pasadena, CA 91101

Distribution List for ARL-TR-78-40 under Contract N00014-76-C-1095 (Cont'd)

Copy No.

30 - 32 San Francisco Area Office
Office of Naval Research
Department of the Navy
760 Market Street, Room 447
San Francisco, CA 94102

33 - 35 Commanding Officer
Office of Naval Research Branch Office
Department of the Navy
495 Summer Street
Boston, MA 02210

36 Office of Naval Research
Department of the Navy
New York Area Office
346 Broadway
New York, NY 10003

Director
U.S. Army Engineering Research and Development Laboratories
Fort Belvoir, VA 22060
37 Attn: Technical Documents Center

38 - 40 ODDR&E Advisory Group on Electronic Devices
201 Varick Street
New York, NY 10014

Air Force Office of Scientific Research
Department of the Air Force
Building 410
Bolling AFB, DC 20332
41 Attn: CAPT W. H. Smith (NAM)

Air Force Weapons Laboratory
Kirtland Air Force Base
Albuquerque, NM 87117
42 Attn: Technical Library

Air Force Avionics Laboratory
Air Force Systems Command
Wright-Patterson Air Force Base
Dayton, OH 45433
43 Attn: Technical Library

Commander
Naval Air Development Center
Department of the Navy
Warminster, PA 18974
44 Attn: Technical Library

Distribution List for ARL-TR-78-40 under Contract N00014-76-C-1095 (Cont'd)

Copy No.

Commander
Naval Weapons Center
Department of the Navy
China Lake, CA 93555
45 Attn: Technical Library (Code 753)
46 Mr. Jack Russell

Commanding Officer and Director
Naval Training Equipment Center
Orlando, FL 32813
47 Attn: Technical Library

New London Laboratory
Naval Underwater Systems Center
New London, CT 06320
48 Attn: Technical Library

Commandant of the Marine Corps
Washington, DC 20380
49 Attn: Scientific Advisor (Code RD-1)

Naval Ordnance Station
Department of the Navy
Indian Head, MD 20640
50 Attn: Technical Library

Superintendent
Naval Postgraduate School
Department of the Navy
Monterey, CA 93940
51 Attn: Technical Library (Code 0212)

Naval Missile Center
Department of the Navy
Point Mugu, CA 93010
52 Attn: Technical Library (Code 5632.2)

Naval Ordnance Station
Louisville, KY 40214
53 Attn: Technical Library

Commanding Officer
Naval Ocean Research & Development Activity
Department of the Navy
NSTL Station, MS 39529
54 Attn: Technical Library

Distribution List for ARL-TR-78-40 under Contract N00014-76-C-1095 (Cont'd)

Copy No.

Naval Explosive Ordnance Disposal Facility
Department of the Navy
Indian Head, MD 20640
55 Attn: Technical Library

Commander
Naval Ocean Systems Center
Department of the Navy
San Diego, CA 92152
56 Attn: Technical Library

Commander
Naval Surface Weapons Center
Dahlgren Laboratory
Department of the Navy
Dahlgren, VA 22448
57 Attn: Technical Library

Commanding Officer
Naval Surface Weapons Center
White Oak Laboratory
Department of the Navy
Silver Spring, MD 20910
58 Attn: Technical Library

Commanding Officer
Naval Ship Research and Development Center
Department of the Navy
Bethesda, MD 20084
59 Attn: Central Library (Code L42 and L43)

Commanding Officer
Naval Avionics Facility
Department of the Navy
Indianapolis, IN 46218
60 Attn: Technical Library

Supply Officer
Naval Coastal Systems Center
Department of the Navy
Panama City, FL 32401
61 Attn: Max Weber (Code 721)

Commanding Officer
Naval Underwater Systems Center
Department of the Navy
New London, CT 06320
62 Attn: Mark Moffett
63 William L. Konrad

Distribution List for ARL-TR-78-40 under Contract N00014-76-C-1095 (Cont'd)

Copy No.

Commanding Officer
Naval Research Laboratory
Department of the Navy
Washington, DC 20375
64 Attn: Anthony I. Eller (Code 8120)

65 - 76 Commanding Officer and Director
Defense Documentation Center
Defense Services Administration
Cameron Station (TC), Building 5
5010 Duke Street
Alexandria, VA 22314

Director
National Bureau of Standards
Washington, DC 20234
77 Attn: Technical Library

Hendrix College
Department of Physics
Conway, AR 72032
78 Attn: Richard Rolleigh

Computer Science Corporation
2251 San Diego Avenue
San Diego, CA 92110
79 Attn: James C. Lockwood

Drittes Physikalische Institut
Universitat Göttingen
Gürgerstrasse 42/44
34 Göttingen
WEST GERMANY
80 Attn: Dr. W. Lauterborn

Lawrence Livermore Laboratory
University of California
P.O. Box 808
Livermore, CA 94550
81 Attn: Dr. W. F. Krupke

Distribution List for ARL-TR-78-40 under Contract N00014-76-C-1095 (Cont'd)

Copy No.

Harry Diamond Laboratories
2800 Powder Mill Road
Adelphi, MD 20783
82 Attn: Technical Library

Brown University
Department of Physics
Providence, RI 02912
83 Attn: Dr. Peter J. Westervelt
84 Dr. Robert T. Beyer

Virginia Polytechnic Institute and State University
Department of Engineering Science and Mechanics
Blacksburg, VA 24061
85 Attn: Dr. A. Nayfeh

University of Rochester
Department of Electrical Engineering
Rochester, NY 14627
86 Attn: Dr. Hugh G. Flynn

87 Office of Naval Research
Resident Representative
Room No. 582, Federal Building
Austin, TX 78701

88 Physical Acoustics Division, ARL:UT

89 Physical Acoustics Group, ARL:UT

90 Robert A. Altenburg, ARL:UT

91 Garland R. Barnard, ARL:UT

92 David T. Blackstock, ARL:UT

93 James R. Clynch, ARL:UT

94 Loyd D. Hampton, ARL:UT

95 C. W. Horton, ARL:UT

96 Thomas G. Muir, ARL:UT

97 Lewis A. Thompson, ARL:UT

Distribution List for ARL TR-78-40 under Contract N00014-76-C-1095 (Cont'd)

Copy No.

98	Magne Vestrheim, ARL:UT
99	Library, ARL:UT
100 - 104	Reserve, ARL:UT